Article

FTO-associated osteoclastogenesis promotes alveolar bone resorption in apical periodontitis male rat via the HK1/USP14/RANK pathway

Yajie Qian[1,5], Jing Wu[2,5], Weidong Yang[1], Ruining Lyu[2], Qiao You[2], Jingjing Li[1], Qin He[1], Yuan Zhuang[1], Wenmei Wang[1] ✉, Yong Wang [2] ✉, Yanan Zhu[1] ✉, Zhiwei Wu [3,4] ✉ & Deyan Chen [2] ✉

Alveolar bone resorption (ABR) is a key pathological manifestation in the development of apical periodontitis (AP) and contributes to the AP-associated tooth loss among AP patients in the clinic. However, the underlying mechanism of ABR development is largely unknown. Here we show, the total levels of N6-methyladenosine (m⁶A) were reduced in AP male rat alveolar bone tissues and BMDM-derived osteoclasts (OC), which was associated with the up-regulation of obesity-associated protein (FTO). Subsequently FTO-mediated hexokinase (HK1) demethylation modification enhancing glycolytic pathway that stabilizes receptor activator of NF-κB (RANK) protein via the deubiquitination activity of ubiquitin-specific protease 14 (USP14), which further promotes osteoclastogenesis to participate in the AP-related ABR development. Finally, Dac51 (an FTO inhibitor) and 2-DG (an HK1 inhibitor) both exhibit the inhibitory activity of osteoclastogenesis. Our current study reveals a molecular mechanism on osteoclastogenesis-related ABR and provides a therapeutic target of AP via modulating the FTO/HK1/USP14/RANK axis.

Apical periodontitis (AP) is an inflammatory disease caused by the infection of the root canal system and a common cause of tooth loss in adults[1]. In addition to the apparent inflammation, periapical alveolar bone resorption (ABR) is also a key pathological manifestation of AP, which is a risk factor for tooth loss[2,3]. Alveolar bone is resorbed by osteoclasts (OC) and renewed by osteoblast[4]. The alveolar bone around the tooth with AP is absorbed with the increased number of OC, and restoration of resorbed alveolar bone to its original condition is very difficult[5]. Therefore, delineating the mechanism of osteoclastogenesis and identifying the targets to mitigate osteoclast-mediated ABR to interrupt AP

development are a key issue that we attempt to address in the current study.

Glycolysis is pivotal for cell proliferation and differentiation and has been demonstrated to be involved in multiple osteoclast-mediated bone resorption diseases via promoting OC proliferation, including rheumatoid arthritis[6,7], etc. Hexokinase (HK), including HK1, HK2, HK3 and HK4, is one of the key enzymes in glycolytic pathways, which is associated with ATP production and metabolite biosynthesis[8]. Unlike HK2-4, HK1 is the most important enzyme for glycolysis, and is ubiquitously expressed and distributed in mammalian tissues[9]. We reported earlier that high-level glycolysis and HK1 expression were

[1]Nanjing Stomatological Hospital, Affiliated Hospital of Medical School, Institute of Stomatology, Nanjing University, Nanjing, China. [2]Medical School of Nanjing University, Nanjing, China. [3]Yunnan Provincial Key Laboratory of Entomological Biopharmaceutical R&D, College of Pharmacy, Dali University, Dali, China. [4]Center for Public Health Research, Medical School of Nanjing University, Nanjing, China. [5]These authors contributed equally: Yajie Qian, Jing Wu. ✉e-mail: wenmei-wang@hotmail.com; yongwang@nju.edu.cn; zh-yanan@163.com; wzhw@nju.edu.cn; chendeyan@nju.edu.cn

present in human clinical AP tissues[10], suggesting that HK1-mediated glycolysis is involved in AP development. Although HK1-mediated glycolysis in regulating the progression of AP inflammation is well established, the relationship between HK1-mediated glycolysis and osteoclastogenesis in ABR of AP is unknown.

N6-methyladenosine (m6A) has been identified as the most abundant and conserved internal modification in eukaryotic RNAs. Glycolysis and HK expression are both regulated by m6A modification[11,12]. Furthermore, m6A modification is associated with osteoclastogenesis and OC-induced bone resorption in osteoporosis[13–15]. Fat mass and obesity-associated protein (FTO) is an eraser of m6A modification and involved in promoting osteoclastogenesis via regulating RNA stability[16–18]. However, the relationships between FTO demethylation and glycolysis regulation in osteoclastogenesis are poorly understood; furthermore, the mechanism of how FTO regulates the glycolysis and its role in the development of osteoclastogenesis-mediated ABR in AP patients remains to be investigated.

The activation of the receptor activator of nuclear factor-κB ligand (RANKL)/RANK signaling pathway has been recognized as a critical event for osteoclastogenesis. After RANKL binds to RANK, multiple signaling pathways are activated by RANK, including nuclear factor of activated T cells (NFATc1), matrix metalloprotein 9 (MMP9), and cathepsin K (CTSK), which directly mediate osteoclastogenesis and osteoclast activation. Therefore, the expression of RANK is essential for the operation of the RNAKL/RANK signaling system. Ubiquitination and deubiquitination can modulate a plethora of physiological processes via regulating the degradation/stabilization of the protein, which requires the involvement of ubiquitinating/deubiquitinating enzymes. The differentiation and maturation of OC are modulated by the ubiquitination and deubiquitination enzymes. It is well-known that RANK expression is increased during osteoclastogenesis. However, the ubiquitination/deubiquitination events of RANK that occurring during osteoclastogenesis are intriguing, and the relationship among FTO, HK1-mediated glycolysis, and RANK during osteoclastogenesis leading to AP-related ABR remains largely unknown.

In the present study, we initially showed that the expression of m6A demethylase FTO expression was upregulated in alveolar bone tissues of experimental rats with AP. Mechanistically, FTO expression promoted HK1 expression to enhance osteoclastogenesis, which was associated with HK1-mediated glycolysis and promoted USP14-midiated RANK deubiquitination modification, further stabilizing RANK expression. By targeting either HK1 using an HK1-specific inhibitor, 2-deoxy-D-glucose (2-DG), or FTO, using an FTO-specific inhibitor, Dac51, the results showed that both inhibitors significantly disrupted osteoclastogenesis, suggesting that FTO/HK1/USP14/RANK axis can serve as a potential therapeutic target for AP-related ABR in the future.

Results
Both rat AP model and BMDM-derived OC model were successfully established
To investigate the underlying mechanisms of the development of AP-associated ABR, we initially established a rat model of AP as shown in Fig. 1a. Micro-CT scanning figures revealed that the periapical radiolucency area in the rat alveolar bone tissue as shown by the sagittal plane (Fig. 1b upper) and the coronal plane (Fig. 1b bottom), respectively. A larger surface area and volume of bone resorption in the alveolar bone tissue of rats with AP were observed in this study (Fig. 1b). The development of ABR is associated with osteoclastogenesis[19], and the number of OC (Fig. 1c-d) and both the mRNA and protein expression of osteoclast-specific markers, including NFATc1, MMP9 and CTSK, were significantly increased in the alveolar bone tissue of AP rats (Fig. 1e, f). Subsequently, we constructed OC derived from the BMDM of C57BL/6 mice as shown in Fig. 1g. The number of OC (Fig. 1h) and both the mRNA

and protein expression of osteoclast-specific markers, including NFATc1, MMP9 and CTSK, in OC were significantly increased at the indicated time periods of 1, 3 and 5 days (Fig. 1i-k). In this study, the number of TRAP-positive cells in the alveolar bone tissues of AP rat were lower, whereas NFATc1, MMP9, and CTSK were still higher at 6 weeks after the rat AP model as compared with that at 3 weeks, which may be associated with the limitation of TRAP assay. TRAP assay only stands for tartrate-resistant acid phosphatase (TRAP), a classical enzyme detectable in OC[20], which is an essential stain capable of detecting OC adhering to the bone resorption line. Consistent with other histochemical stains, the outcome of TRAP staining depends on the complete catabolic center observable in a single microscopic field[21]. At present, a larger surface area and volume of ABR results in a shorter length of bone resorption lines observable in a single microscopic field than earlier times, which may be associated with the reduced number of OC that can be counted in a single microscopic field of view by TRAP staining. In short, all above evidence demonstrated that we successfully constructed the rat AP model and BMDM-derived OC model.

HK1-mediated glycolysis promotes ABR by enhancing osteoclastogenesis
To identify the key functional proteins that were involved in ABR in AP development, we conducted iTRAQ proteomics to investigate the differentially expressed proteins in the alveolar bone tissues of rats with AP. KEGG analysis showed that metabolic pathways were significantly enriched in alveolar bone tissues of rats with AP at 4 weeks (Fig. 2a). We identified that HK1 protein, a key enzyme of glycolysis in the metabolic pathway, exhibited the most significant upward trend ($\log_2FC > 1.5$) (Fig. 2b). Further analysis revealed that the mRNA and protein expression of HK1 were both notably upregulated in time-dependent manner in the alveolar bone tissues of rat AP-related ABR (Fig. 2c–e). Immunohistochemical analysis of an increased HK1 expression in the alveolar bone tissues of rat AP-related ABR (Fig. 2f) was consistent with the analysis of HK1 mRNA and protein in BMDM-derived OC (Fig. 2g, h). Furthermore, higher level of HK1 protein was localized in OC derived from the alveolar bone tissues of AP-related ABR rat and BMDM, respectively (Fig. 2i, j). HK1 is a key enzyme in the glycolytic pathway[22], and we indeed observe a progressively increased level of glucose, lactate, pyruvate, along with the correspondingly increased hexokinase activity in the alveolar bone tissues of AP-related ABR rat model (Fig. 2k). A higher glycolysis level in BMDM-derived OC as compared to the BMDM group as determined by measuring the extracellular acidification rate (Fig. 2l-n). Together, these results demonstrated that HK1-dependent glycolysis was significantly elevated in osteoclastogenesis in the alveolar bone tissues of rats with AP.

Both shHK1 and HK1 inhibitor 2-DG block the osteoclastogenesis in vitro
To further confirm the crucial roles of elevated HK1 levels in the process of osteoclastogenesis, lenti-shHK1 and an HK inhibitor 2-DG[23] were used to inhibit HK1 expression. The expression of HK1 and related biomarkers, such as NFATc1, MMP9 and CTSK, in BMDM-derived OC, were significantly reduced by lenti-shHK1 or 2-DG treatment at a non-cytotoxic concentration (≤0.1 mM) (Fig. 3a–e). Moreover, both lenti-shHK1 and 2-DG treatment reduced the number of OC (Fig. 3f, g) and the bone resorption in a dose-dependent manner (Fig. 3h, i), which was associated with lenti-shHK1 and 2-DG-mediated the reduction of glycolysis level (Fig. 3j, k). These data suggested that targeting HK1 inhibition may also be a powerful 'weapon' to hinder osteoclastogenesis.

Targeting HK1 expression alleviates AP-related ABR in rats
To investigate whether targeting HK1 expression could alleviate ABR in AP rats, rat macrophage-targeted shHK1-GFP delivered via adeno-associated virus (AAV9-shHK1-GFP) and 2-DG were employed in the treatment of the AP-related ABR rats (Fig. 4a). Further, comparing to
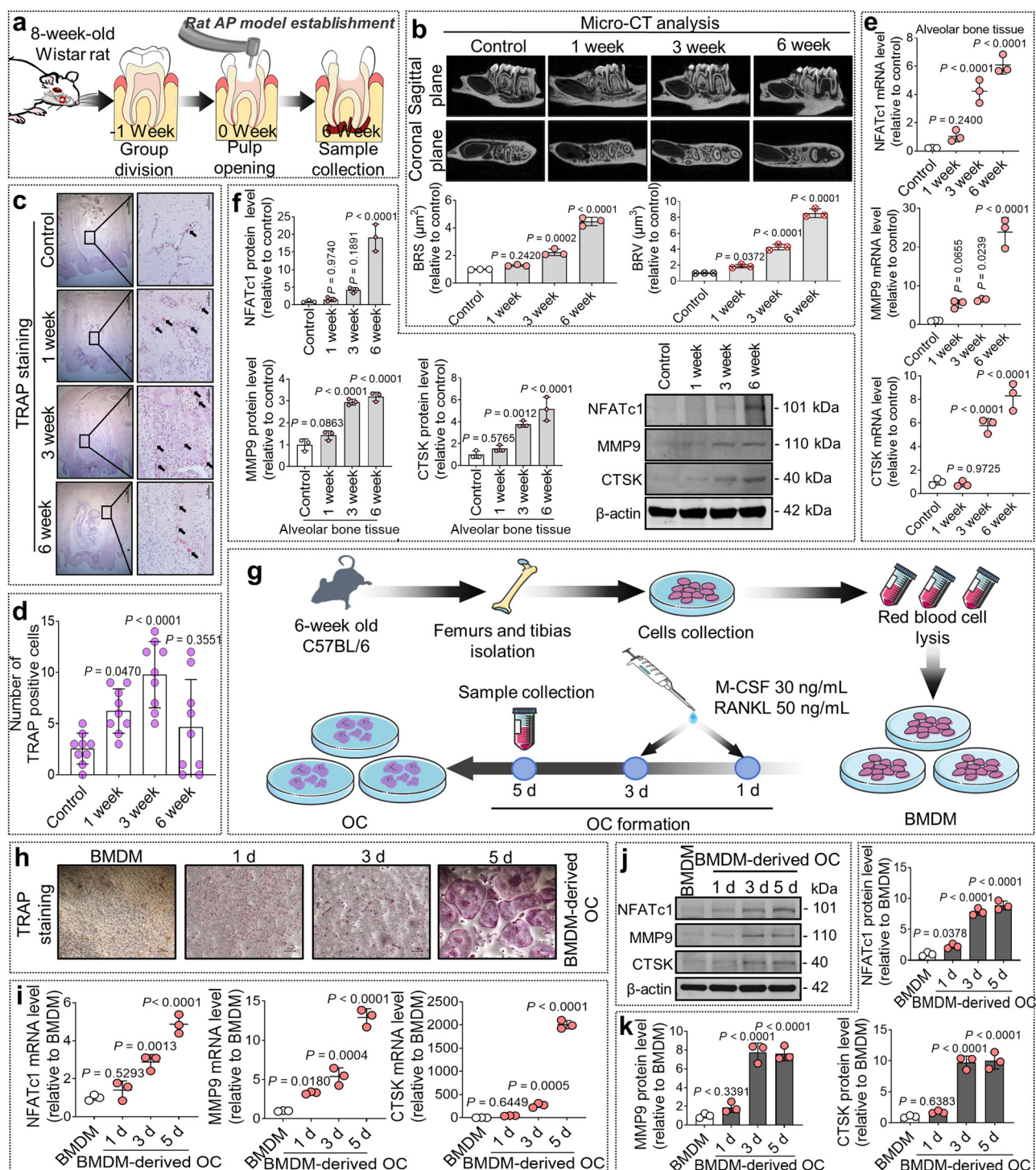
Fig. 1 | BMDM-derived osteoclastogenesis increased in the development of rat AP. a Flow diagram of the construction of apical periodontitis (AP) in rats ($n = 9$ rats per group). **b** The representative micro-CT images of alveolar bone (AB) tissues in the rats with AP ($n = 3$ independent experiments; mean ± SD). The bone resorption fraction was defined as bone resorption surface area (BRS)/bone resorption volume (BRV). **c** Morphometric imaging showed TRAP staining in the AB tissues of rats with AP. Scale bar indicates 1 mm in the left and scale bar indicates 100 μm in the right. Arrowheads pointed the TRAP-positive surfaces ($n = 3$ independent experiments). **d** TRAP-positive multinucleated cells were counted as osteoclast (OC) ($n = 3$ independent experiments with 3 technical replicates; mean ± SD). **e** The mRNA levels of nuclear factor of activated T cells (NFATc1), matrix metalloprotein 9 (MMP9), and cathepsin K (CTSK) in the AB tissues of rats were determined ($n = 3$ independent experiments; mean ± SD). **f** The protein expression in the AB tissues of

rats were determined ($n = 3$ independent experiments; mean ± SD). **g** Flow diagram of the induction of osteoclast in vitro ($n = 3$ mice per group). **h** Representative pictures of TRAP-stained OC. Scale bar indicates 100 μm ($n = 3$ independent experiments). **i** The relative mRNA levels in the process of osteoclastogenesis were determined ($n = 3$ independent experiments; mean ± SD). **j** The protein expression in the process of osteoclastogenesis ($n = 3$ independent experiments). **k** The expression of protein in the process of osteoclastogenesis were determined ($n = 3$ independent experiments; mean ± SD). For the AP rat model, the contralateral teeth served as control. The major statistical procedures applied were: *Shapro–Wiik test* (**b**, **d**, **e**, **f**, **i**, **j**, **k**), *F-test* (**b**, **d**, **k**), *Repeated measures ANOVA* (**b**, **d**), *Kruskal–Wallis H test* and *Dunnett-t test* (**e**, **f**, **i**, **j**, **k**). The statistical test used was two-sided. c (**f**). Source data are available online for this figure.
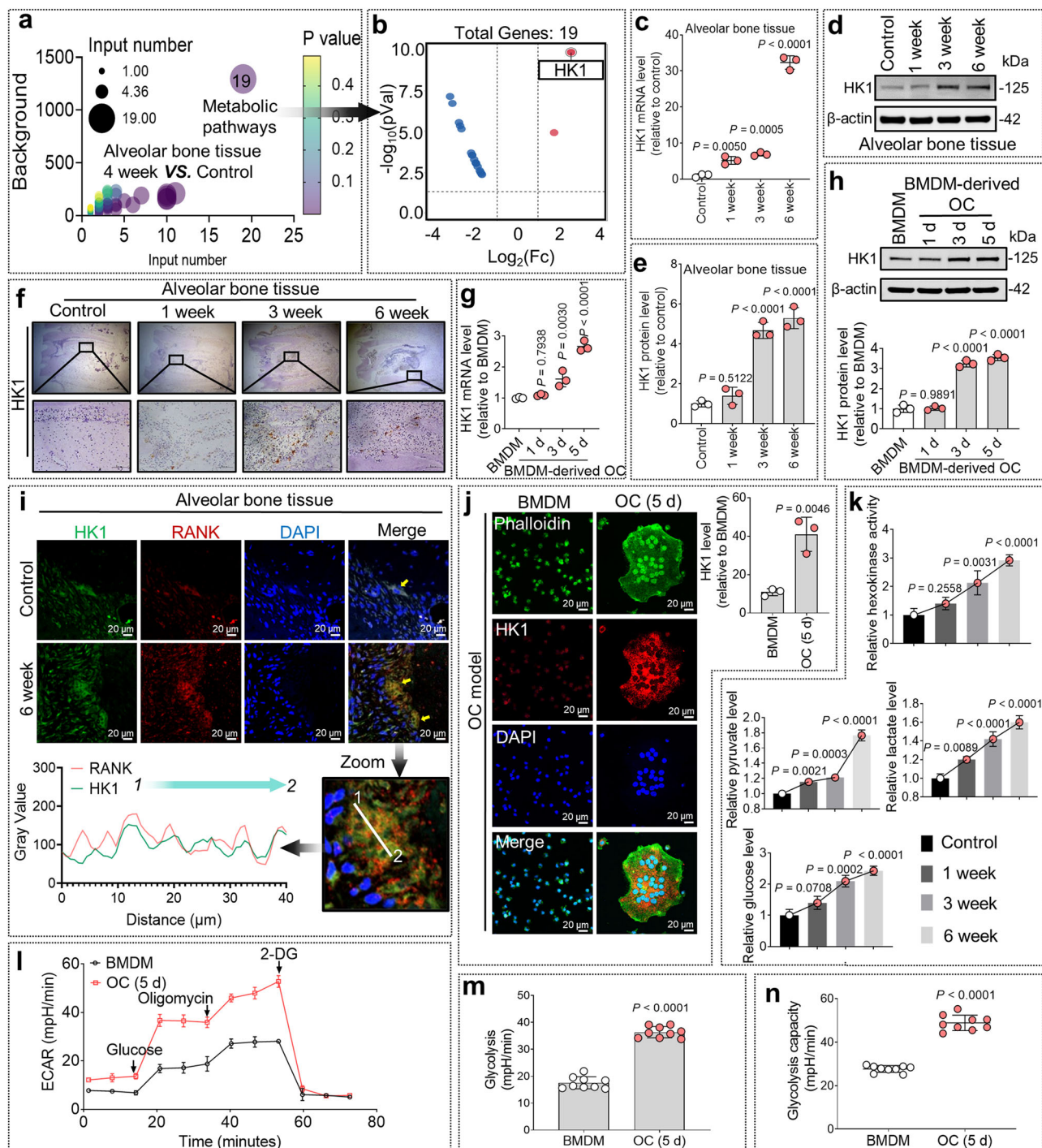
Fig. 2 | HK1-mediated glycolysis promotes ABR by enhancing osteoclastogenesis. a KEGG pathway enrichment analyses of differentially abundant proteins. **b** The differential proteins were enriched in the metabolic pathway. **c** The hexokinase 1 (HK1) mRNA in the alveolar bone (AB) tissues of apical periodontitis (AP) rats was determined ($n = 3$ independent experiments; mean ± SD). **d, e** HK1 protein expression was analyzed in the AB tissues of rats with AP, the relative intensity of bolts ($n = 3$ independent experiments; mean ± SD). **f** Immunohistochemistry analysis of HK1 protein expression in the AB tissues of rats with AP. Scale bar indicates 1 mm in the upper and indicates 100 μm in the bottom ($n = 3$ independent experiments). **g** The HK1 mRNA level in the process of osteoclastogenesis were determined ($n = 3$ independent experiments; mean ± SD). **h** The expression level of HK1 protein expression in the process of osteoclastogenesis were determined ($n = 3$ independent experiments; mean ± SD). **i** The representative images of HK1 (green) and nuclear factor-κB receptor activator (RANK) (red) detection in the AB tissues of rats with AP ($n = 3$ independent experiments). The yellow arrow indicated the colocalization between HK1 and RANK. **j** The representative images of phalloidin (green) and HK1 (red) detection in bone marrow macrophage (BMDM)-derived osteoclast (OC) ($n = 3$ independent experiments; mean ± SD). **k** The levels of glucose, pyruvate, lactate and hexokinase activity were measured ($n = 3$ independent experiments; mean ± SD). **l–n** Measuring the extracellular acidification rate (ECAR) in BMDM-derived OC ($n = 3$ independent experiments with 3 technical replicates; mean ± SD). For the AP rat model, the contralateral teeth served as control. The major statistical procedures applied were: *Shapro–Wiik test* (**a, b, c, d, g, h–k, m**), *F-test* (**a, b, c, d, g, h–k**), *Kruskal–Wallis H test* and *Dunnett-t test* (**c, d, g, h, k**), *Student-t test* (**a, b, i, j, m**). The statistical test used was two-sided. Source data are available online for this figure.
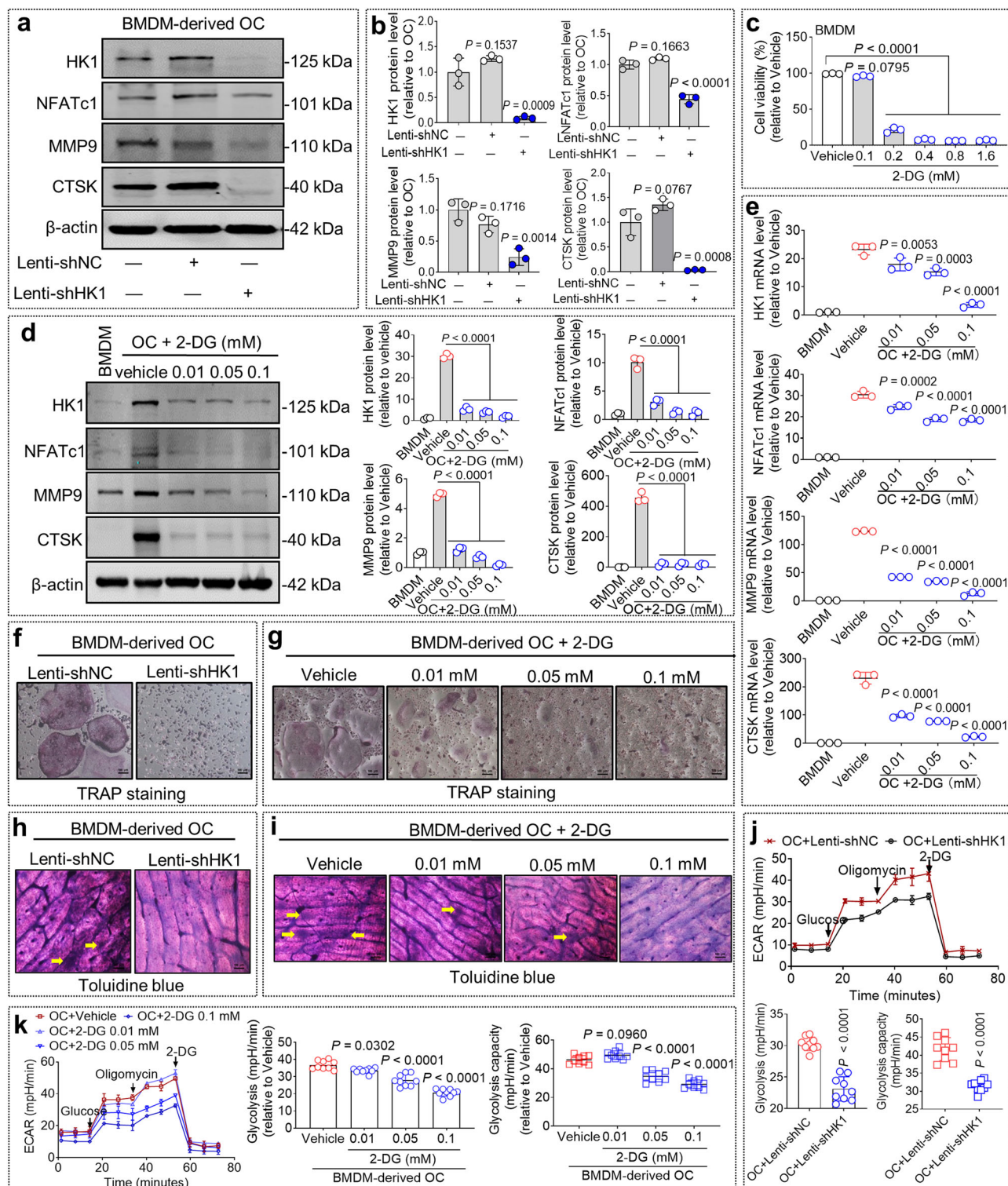
Fig. 3 | Both shHK1 and HK1 inhibitor 2-DG block the osteoclastogenesis in vitro. a, b The level of nuclear factor of activated T cells (NFATc1), matrix metalloprotein 9 (MMP9), and cathepsin K (CTSK) protein in osteoclast (OC) after transfecting for 4 days with lenti-shhexokinase 1 (HK1) were determined (n = 3 independent experiments; mean ± SD). **c** The cell viability of bone marrow macrophage (BMDM) after treatment with 2-DG was measured (n = 3 independent experiments; mean ± SD). **d** The relative protein levels in OC were determined (n = 3 independent experiments; mean ± SD). **e** The mRNA levels in OC after treatment with 2-DG for 4 days were determined (n = 3 independent experiments; mean ± SD). **f, g** The representative TRAP staining images of OC after treatment (n = 3 independent experiments). **h, i** The bone resorption pits on bone slices after treatment with were stained by toluidine blue. Arrowheads indicate the bone resorption (n = 3

independent experiments). **j** The levels of glycolysis in OC were measured by Seahorse XF96 Extracellular Flux Analyzer after transfecting with Lenti-shHK1 for 4 days (n = 3 independent experiments with 3 technical replicates; mean ± SD). **k** Seahorse XF96 Extracellular Flux Analyzer was used to measure the levels of glycolysis in OC after 2-DG treatment at concentrations ranging from 0.01 mM to 0.1 mM for 4 days (n = 3 independent experiments with 3 technical replicates; mean ± SD). BMDM: Bone marrow macrophage, OC: osteoclast. The major statistical procedures applied were: *Shapro–Wiik test* (**b, c, d, e, j, k**), *F-test* (**b, c, d, e, k**), *One-way ANOVA* (**b, c, d, e, k**), *Dunnett-t test* (**b, k**), *SNK-q test* (**c, d, e**), *student-t test* (**j**). The statistical test used was two-sided. Source data are available online for this figure.
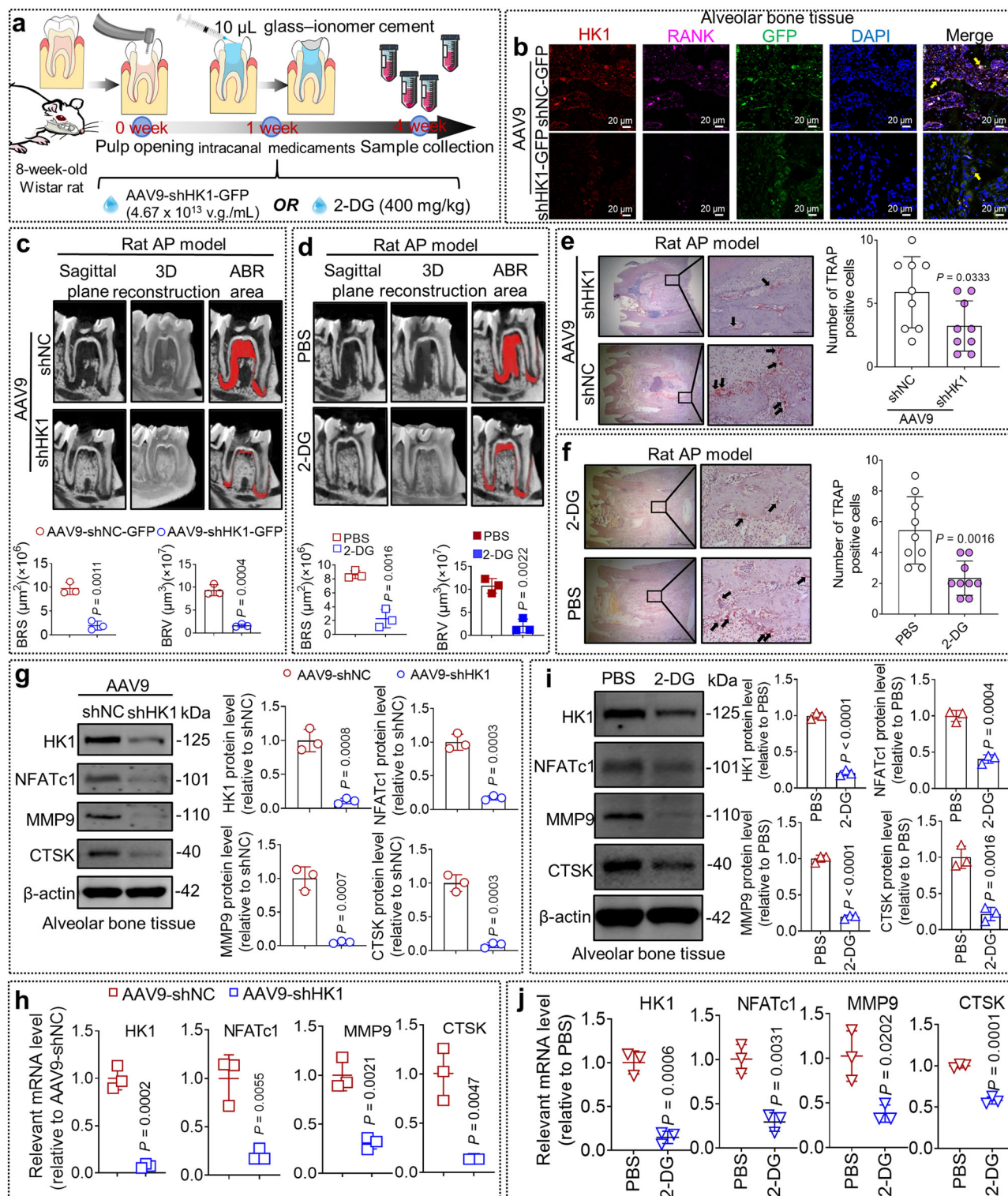
macrophage-targeted AAV9-shNC-GFP, AAV9-shHK1-GFP significantly reduced the expression of HK1 (red) and RANK (pink) in the alveolar bone tissue of AP-related ABR rats (Fig. 4b). AAV9-shHK1-GFP and 2-DG alleviated the expansion of surface area and the volume of bone resorption in the alveolar bone tissue of AP-related ABR rats (Fig. 4c, d). Moreover, the number of OC (Fig. 4e, f), and both the mRNA and protein expression of osteoclast-specific markers, including NFATc1, MMP9 and CTSK, were significantly decreased in the rat alveolar bone tissue of AAV9-shHK1-GFP (Fig. 4g, h) and 2-DG treatment group in rat AP model after 3 weeks (Fig. 4i, j). In summary, HK1 is

a potential therapeutic target for AP-related ABR management, however, the mechanism of HK1 expression upregulation induced in AP-related ABR progression is largely unknown.

FTO upregulation mediates a lower level of m⁶A modification occurring in OC

A previous study showed that m⁶A modification was involved in osteoclastogenesis[14]; however, the roles of m⁶A modification in AP-associated ABR are largely unknown. In rat AP model, we observed a 60-90% reduction of total m⁶A in the alveolar bone tissue with the

Fig. 4 | Targeting HK1 by AAV9-shHK1-GFP and 2-DG both alleviated the ABR in the rat AP model. a Flow diagram of the treatment of apical periodontitis (AP) with the macrophage-targeted AAV9-shHK1-GFP (4.67 ×10^{11} v.g/rat, 10 μL/rat) or 2-DG (400 mg/kg) in rats (*n* = 9 rats per group). **b** The representative images of hexokinase 1 (HK1) (red) and nuclear factor-κB receptor activator (RANK) (pink) detection in the alveolar bone (AB) tissues of rats (*n* = 3 independent experiments). **c** The representative micro-CT images of AB tissues of the rats (*n* = 3 independent experiments; mean ± SD). The bone resorption fraction was defined as bone resorption surface area (BRS)/bone resorption volume (BRV). **d** The representative micro-CT images of AB tissues of rats (*n* = 3 independent experiments with 3 technical replicates; mean ± SD). The bone resorption fraction was defined as bone resorption surface area (BRS) (mm²)/bone resorption volume (BRV) (mm³). **e**, **f** Morphometric imaging showed TRAP staining in the AB tissues of rats (*n* = 3 independent experiments with 3 technical replicates; mean ± SD). Scale bar indicates 1 mm in the left and scale bar indicates 100 μm in the right. Arrowheads pointed the TRAP-positive surfaces. TRAP-positive multinucleated cells were counted as OC. **g**, **h** The mRNA and protein levels of HK1, nuclear factor of activated T cells (NFATc1), matrix metalloprotein 9 (MMP9), and cathepsin K (CTSK) in the AB tissues of rats were determined (*n* = 3 independent experiments; mean ± SD). **i** The level of relevant protein in the AB tissues of rats were determined (*n* = 3 independent experiments; mean ± SD). **j** The mRNA levels in the AB tissues of rats were determined (*n* = 3 independent experiments; mean ± SD). The AAV9-shNC group AP rats were received the treatment of unedited plasmid carried by AAV9 vector; the PBS group AP rats were treated with PBS, a solvent for 2-DG. The major statistical procedures applied were: *Shapro–Wiik test* (**c**, **d**, **e**–**j**), *F-test* (**i**), *student-t test* (**c**, **d**, **e**–**h**, **j**), *Wilcoxon test* (**g**, **h**, **j**), *Kruskal–Wallis H test* and *Dunnett-t test* (**i**). The statistical test used was two-sided. Source data are available online for this figure.

development of AP at the indicated time periods of 1, 3, and 6 weeks (Fig. 5a). And the total level of m⁶A modification was also reduced in OC at 1, 3, 5 days (Fig. 5b). These results suggested that a significant reduction of total m⁶A was associated with osteoclastogenesis, implicating the important roles of m⁶A was involved in the development of ABR in rat AP model. The reduction of m⁶A modification levels is usually associated with demethylase expression[24]; therefore, we subsequently measured the expression of FTO and ALKBH5, two molecules that are well-known to modulate m⁶A demethylation, in the alveolar bone tissues of AP rat with ABR[25]. As expected, the protein and mRNA levels of FTO and ALKBH5 were significantly upregulated in both alveolar bone tissues of AP rat with ABR (Fig. 5c, d) and BMDM-derived OC (Fig. 5e, f) in a time-dependent manner, which implying that FTO and ALKBH5 were both involved in the ABR development via modulating demethylation modification. Compared with ALKBH5, FTO showed a significantly higher and earlier expression in OC of the AP rat model, suggesting a potentially more important role of FTO in ABR development (Fig. 5c, e). Therefore, we further focused on the role of FTO expression in AP-related ABR development, and observed that the level of FTO protein expression in BMDM-derived OC were higher than its expression in BMDM (Fig. 5g). Moreover, FTO (green) primarily expressed in OC (marked by RANK antibody, red) of the rat AP model (Fig. 5h). In summary, FTO expression mediated a lower level of m⁶A modification might participate in the development of AP-related ABR.

Both shFTO and an FTO specific inhibitor Dac51 reduces the osteoclastogenesis in vitro

To determine the role of FTO during the process of osteoclastogenesis, BMDMs were treated with lenti-shFTO, or Dac51 (a specific inhibitor of FTO)[26], when they were induced from BMDM-derived OC. Lenti-shFTO significantly increased the total level of m⁶A in BMDM-derived OC (Fig. 6a). Dac51, an FTO inhibitor, at non-cytotoxic concentrations also increased the total level of m⁶A in BMDM-derived OC (Fig. 6b, c). Both lenti-shFTO and Dac51 treatment inhibited FTO protein expression with a downregulation of the protein expression of osteoclast specific markers, including NFATc1, MMP9 and CTSK (Fig. 6d, e). Additionally, treatment with lenti-shFTO or Dac51 decreased the quantity of OC (Fig. 6f, g) and their bone-resorption capacity in BMDM-derived OC (Fig. 6h, i). Collectively, decreased levels of FTO expression following lenti-shFTO or Dac51 reduced the osteoclast formation, suggesting that targeting FTO could potentially alleviate the progression of ABR in AP by impeding osteoclastogenesis.

Targeting FTO expression alleviates AP-related ABR in rats

To investigate whether targeting FTO could alleviate ABR in rat AP model, rat macrophage-targeted shFTO-GFP delivered via adeno-associated virus (AAV9-shFTO-GFP) and Dac51 were employed in the treatment of the rat AP-related ABR, respectively (Fig. 7a). Further, comparing to macrophage-targeted AAV9-shNC-GFP, AAV9-shFTO-GFP significantly reduced the expression of FTO (red) and RANK (pink) in the alveolar bone tissues of AP-related ABR rats (Fig. 7b). Interestingly, both AAV9-shFTO and Dac51 alleviated the expansion of surface area and the volume of bone resorption in the alveolar bone tissue of AP-related ABR rats (Fig. 7c, d). Moreover, AAV9-shFTO-GFP and Dac51 reduced the number of OC in the alveolar bone tissues of AP-related ABR rats at 4 weeks (Fig. 7e, f). Importantly, both AAV9-shFTO-GFP and Dac51 treatment also increased the total level of m⁶A in the rat alveolar bone tissues of AP model after 3 weeks (Fig. 7g, h). Additionally, both AAV9-shFTO-GFP and Dac51 treatment reduced the protein and mRNA expression of osteoclast-specific markers, including NFATc1, MMP9 and CTSK, in the rat alveolar bone tissue of AAV9-shFTO and Dac51 treatment group (Fig. 7i, j and Supplementary Fig.1a, b) after 3 weeks. In summary, FTO, who is similar to HK1, is also a potential therapeutic target for the AP-related ABR management, however, the relationship between FTO and HK1 in AP-related ABR progression is largely unknown.

FTO promotes osteoclastogenesis by enhancing HK1 expression and HK1-mediated glycolysis

Almost all mRNAs of mammalian genes can be regulated by m⁶A modification, including those encoding key enzymes in glycolysis pathway[27]. m⁶A-enriched RNA from the alveolar bone tissues of rat AP-related ABR showed that the level of m⁶A modification on HK1 transcription level was significantly lower than that in the control group (Fig. 8a). And the RIP results revealed that FTO directly interacted with HK1 mRNA in the AP rats alveolar bone tissues and BMDM-derived OC (Fig. 8b, c), which implied that FTO may upregulate HK1 expression through modulating m⁶A demethylation modification on HK1 mRNA. As expected, we further found that FTO overexpression notably upregulated HK1 protein expression in HEK-293T cells (Fig. 8d), while both lenti-shFTO knockdown and an FTO inhibitor Dac51 treatment inhibited the expression of HK1 protein in BMDM-derived OC (Fig. 8e, f). m⁶A methylation/demethylation modification has been recognized to regulate gene expression by modulating the target gene mRNA stability[17], and we observed that the stability of HK1 mRNA was enhanced in FTO-overexpressed-HEK-293T cells during the treatment of actinomycin D (Fig. 8g). In order to investigate the relationship between FTO and HK1-mediated glycolysis, ECAR and OCR assay were performed in BMDM-derived OC, and we found that lenti-shFTO transfection or Dac51 treatment both decreased the levels of HK1-meidated glycolysis, and Lenti-shFTO transfection increased the maximal respiration in the BMDM-derived OC (Fig. 8h–j), which implied that FTO inhibition increased energy requirements during osteoclastogenesis, suggesting an inadequate energy supply, while FTO upregulation facilitated HK1-mediated glycolysis during osteoclastogenesis, which contributes to energy supply during osteoclastogenesis. In short, our findings suggest that FTO plays a positive role in regulating glycolysis by stabilizing HK1 mRNA through FTO-catalyzed demethylation, thereby enhancing osteoclastogenesis.
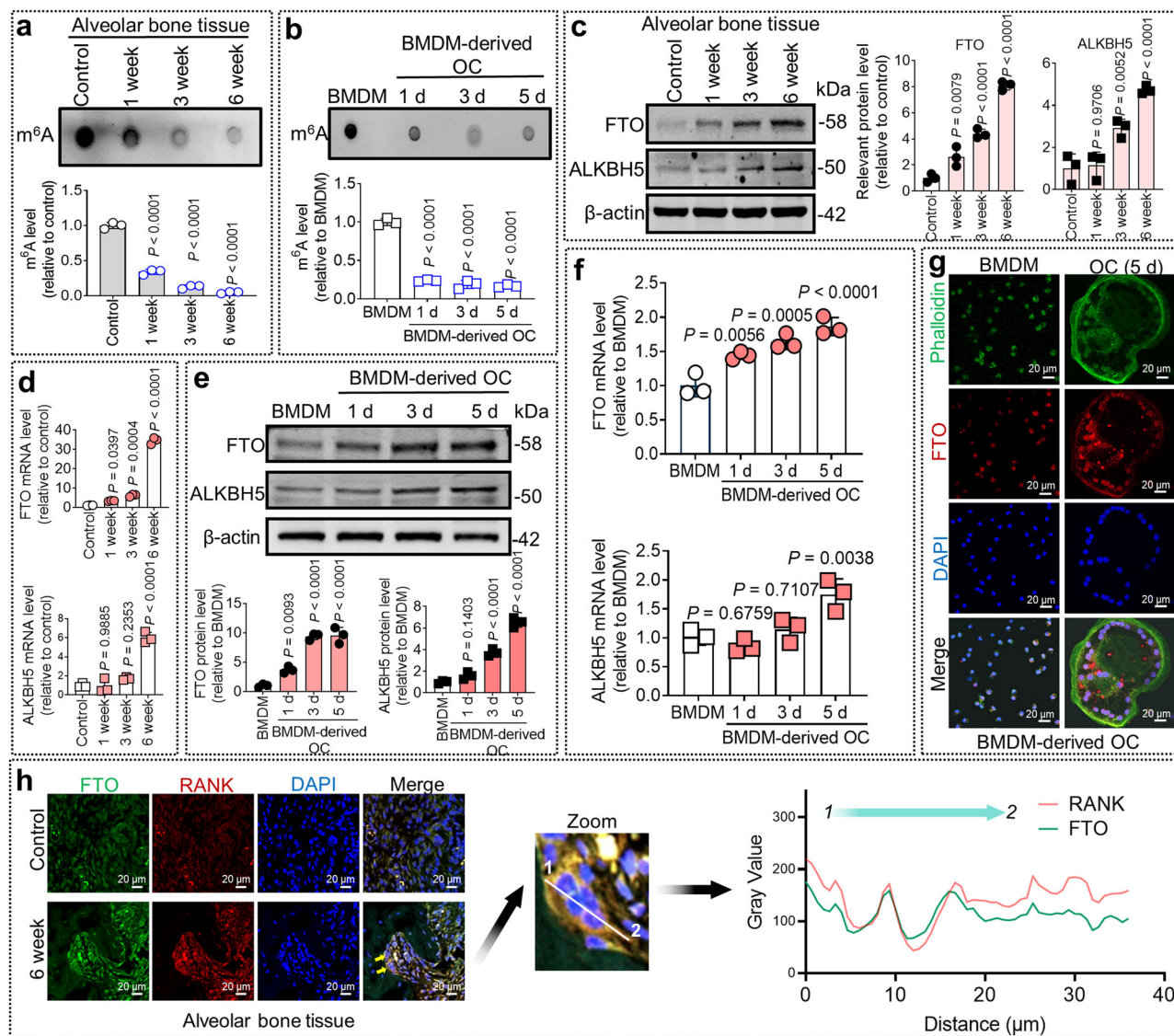
Fig. 5 | m⁶A demethylases FTO and ALKBH5 were both increased in alveolar bone tissues of AP rats and OC, respectively. a The total m⁶A methylation level in the alveolar bone (AB) tissues of rats with AP was measured ($n = 3$ independent experiments; mean ± SD). **b** The total m⁶A methylation level was measured ($n = 3$ independent experiments; mean ± SD). **c** Immunoblotting of obesity-associated protein (FTO) and Alk B homologous protein 5 (ALKBH5) expression in the AB tissues of rats with AP. The expression levels of FTO and ALKBH5 were determined ($n = 3$ independent experiments with 3 technical replicates; mean ± SD). **d** *FTO* mRNA levels of and *ALKBH5* gene in the AB tissues of rats with AP were determined ($n = 3$ independent experiments; mean ± SD). **e** Immunoblotting of FTO and ALKBH5 expression during osteoclastogenesis. The expression level of FTO and ALKBH5 protein during osteoclastogenesis were determined ($n = 3$ independent experiments; mean ± SD). **f** *FTO* and *ALKBH5* mRNA levels during

osteoclastogenesis were determined ($n = 3$ independent experiments; mean ± SD). **g** Representative images of phalloidin (green) and FTO (red) detection by immunofluorescence in bone marrow macrophage (BMDM)-derived osteoclast (OC) at 5 days ($n = 3$ independent experiments). **h** Representative images of FTO (green) and nuclear factor-κB receptor activator (RANK) (red) detection by immunofluorescence in the AB tissues of rats with AP at 6 weeks and in the control group ($n = 3$ independent experiments). Fiji software was used to assessed the intensity of colocalization. Fluorescence intensity profiles of positive cells showed different colocalized signals of endogenous FTO and RANK. For the AP rat model, the contralateral teeth served as control. The major statistical procedures applied were: *Shapro–Wiik test* (**a–g**), *F-test* (**a–f**), *Repeated measures ANOVA* and *Dunnett-t test* (**a–f**), *student-t test* (**g**). The statistical test used was two-sided. Source data are available online for this figure.

The upcoming study will delve deeper into the molecular mechanism underlying the FTO/HK1 pathway's impact on osteoclastogenesis.

FTO/HK1 signal pathway regulates osteoclastogenesis through stabilizing RANK protein expression

RANK, a receptor, who is highly expressed on osteoclast precursors, plays a crucial role in osteoclastogenesis. Upon binding with RANKL, RANKL/RANK signaling triggers and enhances the process of osteoclastogenesis[28,29]. In this study, endogenous RANK protein and mRNA were steadily increased at days 3 and 5 during osteoclastogenesis

(Fig. 9a, b), while the endogenous RANK protein expression was significantly reduced in lenti-shFTO knockdown BMDM-derived OC (Fig. 9c). Furthermore, AAV9-shFTO-GFP treatment also reduced the endogenous expression of HK1 and RANK protein in the rat alveolar bone tissues of rat AP model after 3 weeks (Fig. 9d, e). Subsequently, we would like to investigate whether RANK was dependent on the triggering of the FTO/HK1 signaling pathway. We initially excluded a direct regulatory effect of FTO on RANK expression. Although RIP results showed an interaction between FTO and RANK mRNA in BMDM-derived osteoclasts (Fig. 9f); however, the exogenous RANK protein was
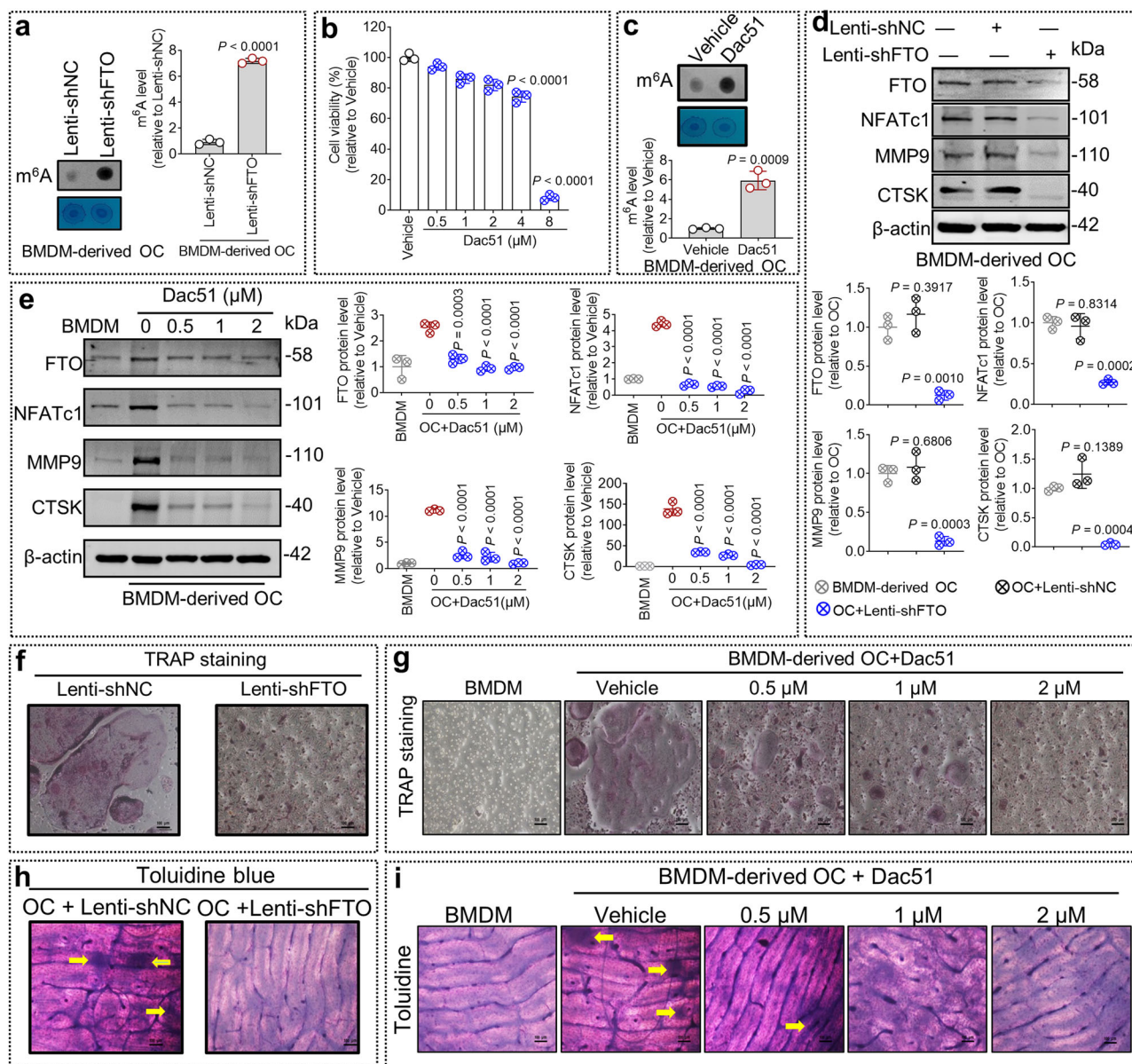
Fig. 6 | m⁶A demethylase FTO was involved in the osteoclastogenesis. a The total m⁶A methylation level in osteoclast (OC) with obesity-associated protein (FTO) shRNA transfection using Lentiviral vectors was measured ($n = 3$ independent experiments; mean ± SD). **b** The cell viability of bone marrow macrophage (BMDM) after treatment with Dac51 (0, 0.5, 1, 2, 4 and 8 μM) was measured ($n = 3$ independent experiments; mean ± SD). **c** The total m⁶A methylation level in OC after treatment with Dac51 (2 μM) was measured ($n = 3$ independent experiments; mean ± SD). **d** The relative protein levels of FTO, nuclear factor of activated T cells (NFATc1), matrix metalloprotein 9 (MMP9), and cathepsin K (CTSK) in OC with Lenti-shFTO and Lenti-shNC transfection were determined ($n = 3$ independent experiments; mean ± SD). **e** The relative protein levels in OC after treatment with Dac51 were determined ($n = 3$ independent experiments; mean ± SD). **f** The representative TRAP staining images of OC were shown after transfecting with Lenti-shFTO and Lenti-shNC for 4 days, respectively ($n = 3$

independent experiments). **g** The representative TRAP staining images of OC after treatment with Dac51 for 4 days at different concentrations were shown ($n = 3$ independent experiments). **h** The bone resorption pits on bone slices after transfecting with Lenti-shFTO as compared to Lenti-shNC for 4 days were stained by toluidine blue. The arrowheads marked in yellow color indicate the bone resorption pits ($n = 3$ independent experiments). Scale bar indicates 100 μm. **i** The bone resorption pits on bone slices after treatment with Dac51 for 4 days were stained by toluidine blue ($n = 3$ independent experiments). Arrowheads indicate the bone resorption pits. The Lenti-shNC group BMDM cells were received the treatment of unedited plasmid carried by lentiviral vector. The major statistical procedures applied were: *Shapro–Wiik test* (**a**–**e**), *F-test* (**b**, **d**, **e**), *Student-t test* (**a**, **c**), *One-way ANOVA* and *Dunnett-t test* (**d**, **e**), *Kruskal–Wallis H test* and *Dunnett-t test* (**d**, **e**). The statistical test used was two-sided. Source data are available online for this figure.

only upregulated in FTO and HK1 co-transfection HEK-293T cells, while transfection with either FTO or HK1 alone did not produce the same effect (Fig. 9g). The above results indicating that RANK expression is not directly regulated by either FTO or HK1 alone. Secondly, we excluded a direct regulatory effect of HK1 on RANK expression. PKM2-IN-1 is a specific inhibitor for PKM2, a downstream molecule of HK1 that co-regulates the glycolysis with HK1, significantly abolished the expression of HK1 overexpression induced the exogenous RANK protein

expression (Fig. 9h), which implied that HK1-induced RANK expression dependent on HK1-mediated glycolysis, but not the direct action of HK1. Finally, we investigated whether HK1-mediated glycolysis regulates RANK de novo synthesis, and found that either lenti-shHK1 transfection or 2-DG treatment reduced RANK protein level in the BMDM-derived osteoclasts (Fig. 9i, k); however, both lenti-shHK1 transfection or 2-DG ≥0.01 mM treatment did not affect the level of RANK mRNA in the BMDM-derived osteoclasts (Fig. 9j, l). We further confirmed the result
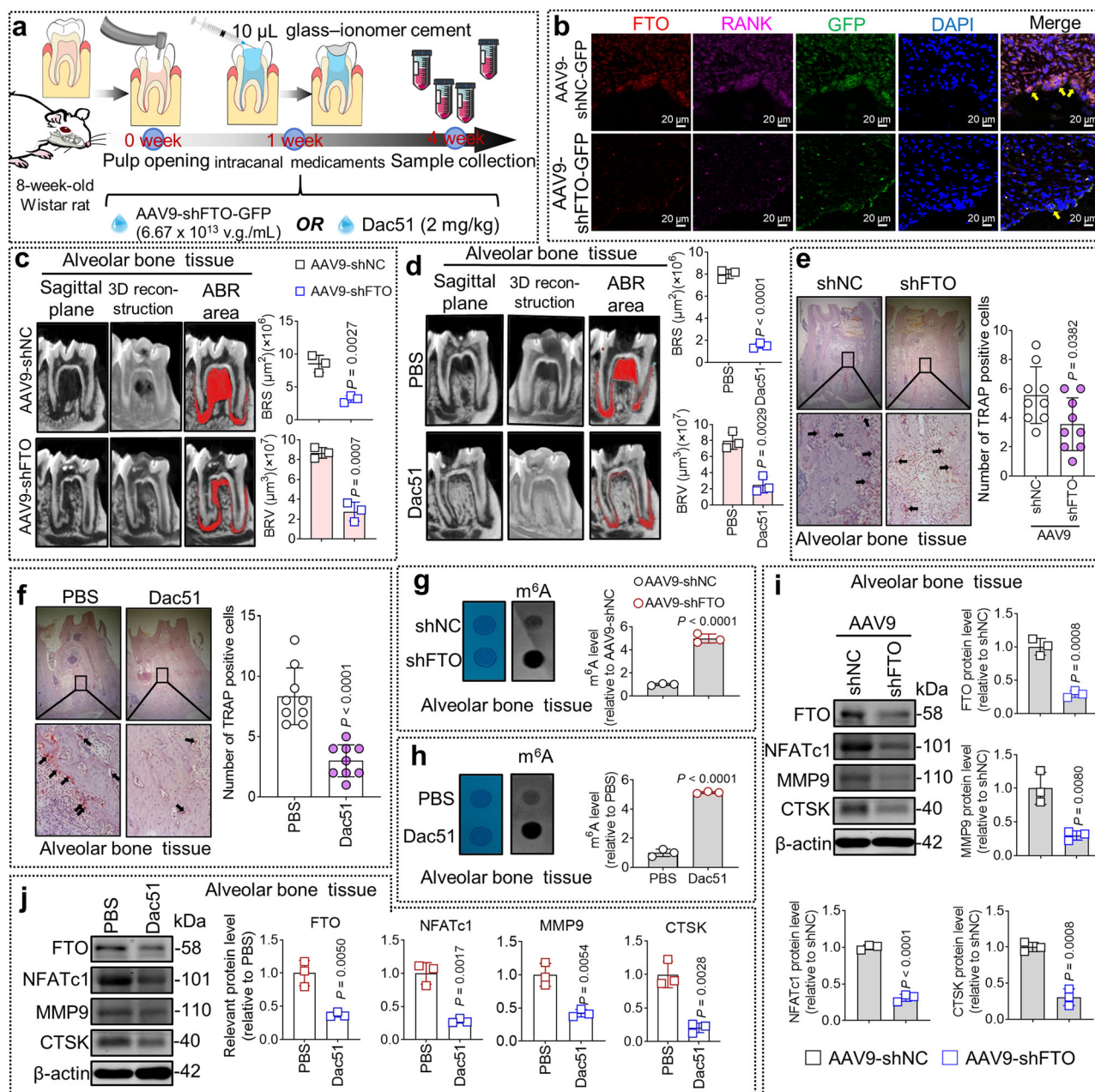
Fig. 7 | Targeting FTO by AAV9-shFTO-GFP and Dac51 both alleviated the ABR in the rat AP model. a Flow diagram of the treatment of apical periodontitis (AP) with the macrophage-targeted AAV9-shFTO-GFP (6.67×10^{11} v.g./rat, 10 μL/rat) or Dac51 (2 mg/kg) in rats, respectively ($n = 9$ rats per group). **b** The representative images of obesity-associated protein (FTO) (red) and nuclear factor-κB receptor activator (RANK) (pink) detection in the alveolar bone (AB) tissues of rats ($n = 3$ independent experiments). **c** The representative micro-CT images of AB tissues in the rats ($n = 3$ independent experiments; mean ± SD). The bone resorption fraction was defined as bone resorption surface area (BRS)/bone resorption volume (BRV). **d** The representative micro-CT images of AB tissues in the rats with AP ($n = 3$ independent experiments; mean ± SD). **e** Morphometric imaging showed TRAP staining in the AB tissues of rats with AP ($n = 3$ independent experiments with 3 technical replicates; mean ± SD). Arrowheads pointed the TRAP-positive surfaces. TRAP-positive multinucleated cells were counted as OC. **f** Morphometric imaging

showed TRAP staining in the AB tissues of rats with AP ($n = 3$ independent experiments with 3 technical replicates; mean ± SD). **g** The total m^6A methylation level in the AB tissues of rats ($n = 3$ independent experiments; mean ± SD). **h** The total m^6A methylation level in the AB tissues of rats was measured ($n = 3$ independent experiments; mean ± SD). **i** The expression level of the relevant protein in the AB tissues of rats were determined ($n = 3$ independent experiments; mean ± SD). **j** The relevant protein level of in the AB tissues of rats with AP were determined ($n = 3$ independent experiments; mean ± SD). The AAV9-shNC group AP rats were received the treatment of unedited plasmid carried by AAV9 vector; the PBS group AP rats were treated with PBS, a solvent for Dac51. The major statistical procedures applied were: *Shapro–Wiik test* (**c–j**), *F-test* (**j**), *Student-t test* (**c–h**), *Wilcoxon test* (**i**), *Kruskal–Wallis H test* and *Dunnett-t test* (**j**). The statistical test used was two-sided. Source data are available online for this figure.

that AAV9-shHK1-GFP reduced the RANK protein level in the rat alveolar bone tissues of AP model after 3 weeks (Fig. 9m), which was consistent with the result in Fig. 9i. The above results suggested that interruption of glycolysis by targeting HK1 affected RANK at a post-translational step rather than a de novo synthesis.

FTO/HK1 stabilizes RANK protein via USP14-mediated de-ubiquitination of RANK in BMDM-derived osteoclasts
Ubiquitination, the most common form of post-translational modification, serves a crucial role in the regulation of cellular functions via modulating the degradation of cellular proteins[30]. At present, FTO/HK1
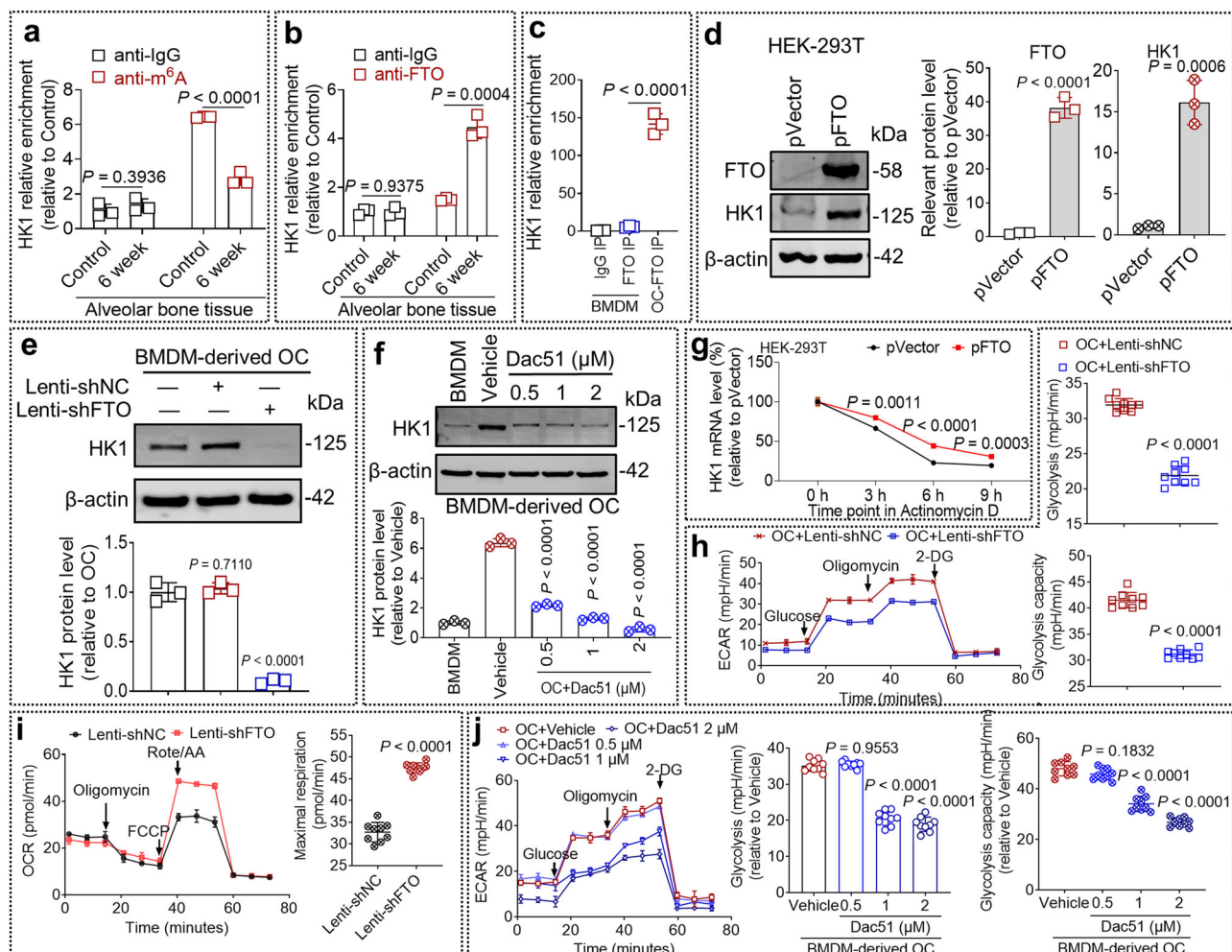
Fig. 8 | Demethylase FTO mediated m⁶A demethylation modification of HK1.
a m^{6}A enrichment on *hexokinase 1* (*HK1*) mRNAs in the alveolar bone (AB) tissues of rats. The IgG antibody was served as a negative control ($n = 3$ independent experiments; mean ± SD). **b** The interplay between obesity-associated protein (FTO) and HK1 was measured in the AB tissues of rats. The IgG antibody was served as a negative control ($n = 3$ independent experiments; mean ± SD). **c** The interplay between FTO and HK1 was measured in bone marrow macrophage (BMDM)-derived osteoclast (OC). The IgG antibody was served as a negative control ($n = 3$ independent experiments; mean ± SD). **d** The relative protein levels in 293T cells were determined ($n = 3$ independent experiments; mean ± SD). **e** The relative protein levels of HK1 in OC were determined ($n = 3$ independent experiments; mean ± SD). **f** The HK1 protein levels in OC after treatment with Dac51 were determined ($n = 3$ independent experiments; mean ± SD). **g** The mRNA stability of *HK1* after FTO overexpression in 293 T cells was detected ($n = 3$ independent experiments with 3 technical replicates; mean ± SD). **h** Measuring the levels of glycolysis in OC ($n = 3$ independent experiments with 3 technical replicates; mean ± SD). **i** The levels of the mitochondrial activity in OC by oxygen consumption rate (OCR) ($n = 3$ independent experiments with 3 technical replicates; mean ± SD). **j** The levels of glycolysis in OC after Dac51 treatment by extracellular acidification rate (ECAR) ($n = 3$ independent experiments with 3 technical replicates; mean ± SD). For the AP rat model, the contralateral teeth served as control. The Lenti-shNC group BMDM cells were received the treatment of unedited plasmid carried by lentiviral vector. The major statistical procedures applied were: *Shapro–Wiik test* (**a**–**j**), *F-test* (**b**, **d**, **e**, **f**, **h**, **j**), *paired t test* (**a**), *Student-t test* (**c**, **g**, **i**), *One-way ANOVA* and *Dunnett-t test* (**d**, **e**, **f**, **h**, **j**). The statistical test used was two-sided. Source data are available online for this figure.

pathway stabilized RANK protein during osteoclastogenesis, which may be associated with de-ubiquitination of RANK. We detected a reduction of total ubiquitin level in BMDM-derived OC, while 2-DG treatment partially reversed the total ubiquitin level (Fig. 10a). MG132, a specific inhibitor for the proteasome pathway[31], not only abolished the degradation of RANK protein induced by 2-DG, but also rescued the expression of OC markers, such as NFATc1, MMP9, and CTSK (Fig. 10b). USP14, a deubiquitinating enzyme that regulates the stability and the activity of target proteins, who is highly expressed in macrophages[32,33]. In our study, although the expression of USP14 did not change during the dynamic formation of OC, the co-localization frequency of RANK and USP14 was gradually increased (Fig. 10c) in BMDM-derived OC. Co-IP assay further showed that the interaction activity of USP14 and RANK in BMDM-derived osteoclasts was higher than in the group of BMDM (Fig. 10d). Interestingly, the interaction of

exogenous RANK and exogenous USP14 was dependent on HK1 over-expression in HEK-293T cells (Fig. 10e). Collectively, these data suggested that HK1 stabilized RANK protein by USP14-mediated the inhibition of proteasome pathway, which might contribute to the process of the osteoclastogenesis in AP-related ABR.

Discussion

ABR is a key pathological manifestation in the development of AP and contributes to the AP-associated tooth loss. Therefore, the attempts to elucidate the mechanism of ABR development are essential to understand the pathogenesis and develop the new therapeutic interventions. At present, our study showed that the reduction of total m⁶A level occurred in the rat alveolar bone tissues of AP-related ABR, which was associated with FTO upregulation. Subsequently, FTO-mediated m⁶A demethylation enhanced the glycolysis level via stabilizing HK1
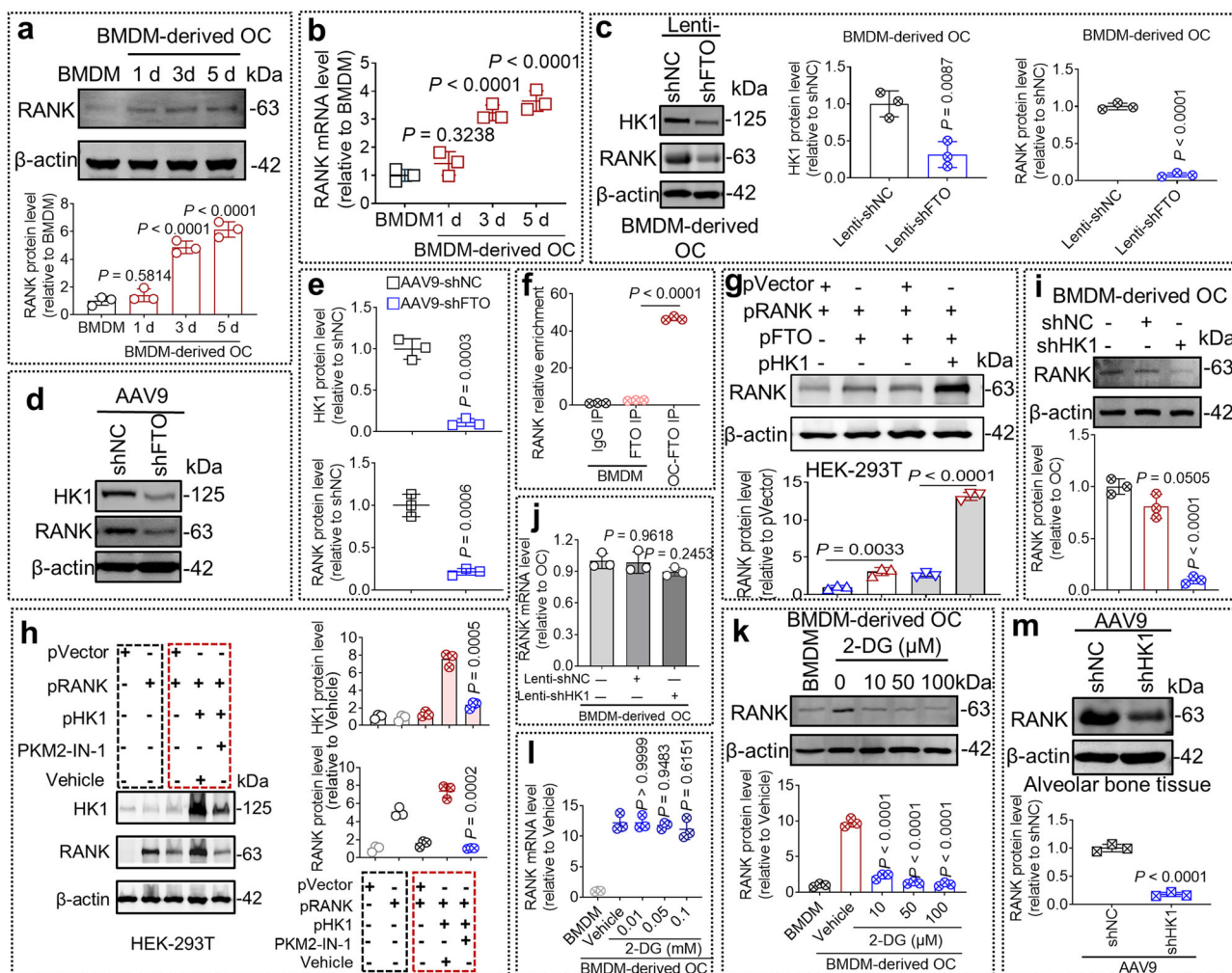
Fig. 9 | HK1 upregulation promoted osteoclastogenesis by stabilizing RANK protein expression. a The relative protein in bone marrow macrophage (BMDM)-derived osteoclast (OC) was determined (n = 3 independent experiments; mean ± SD). **b** The relative mRNA in OC was determined (n = 3 independent experiments; mean ± SD). **c** The protein expressed in OC cells (n = 3 independent experiments; mean ± SD). **d** The relative protein expression in the AB tissues of apical periodontitis (AP) rats (n = 3 independent experiments). **e** The intensity of the blots were analyzed (n = 3 independent experiments; mean ± SD). **f** The interplay between obesity-associated protein (FTO) and nuclear factor-κB receptor activator (RANK) was measured by RIP assay. The IgG antibody was served as a negative control (n = 3 independent experiments; mean ± SD). **g** The relative protein in 293 T cells overexpressing RANK for 24 h was determined (n = 3 independent experiments; mean ± SD). **h** The relative protein in 293T cells with hexokinase 1 (HK1) overexpression followed by PKM2-IN-1 (5 μM, MCE) was detected (n = 3 independent

experiments; mean ± SD). **i** The relative protein in OC was determined (n = 3 independent experiments; mean ± SD).**j** The relative mRNA level in OC was determined (n = 3 independent experiments; mean ± SD). **k** The relative protein in OC after treatment with 2-DG was determined (n = 3 independent experiments; mean ± SD). **l** The relative mRNA in OC after treatment with 2-DG were determined (n = 3 independent experiments; mean ± SD). **m** The relative protein in the AB tissues were determined (n = 3 independent experiments; mean ± SD). The Lenti-shNC group BMDM cells and the AAV9-shNC group AP rats were received the treatment of unedited plasmid carried by lentiviral vector and AAV9 vector, respectively. The major statistical procedures applied were: *Shapro–Wiik test* (**a–m**), *F-test* (**a, b, f–l**), *Student-t test* (**c, e, m**), *Repeated measures ANOVA* and *Dunnett-t test* (**a**), *One-way ANOVA* and *Dunnett-t test* (**f–k**). The statistical test used was two-sided. Source data are available online for this figure.

mRNA expression. Increased glycolysis, orchestrated by the FTO/HK1 pathway, promotes the de-ubiquitination of RANK mediated by USP14, which stabilizes RANK protein expression and ultimately increases the development of osteoclastogenesis of AP-related ABR.

The intracellular metabolic pathways are involved in the development of multiple diseases[34,35]. Glycolysis is considered to be one of the important intracellular metabolic pathways, which participates in cell proliferation and differentiation by providing ATP[36]. Increased glycolysis was involved in the process of osteoclastogenesis, which had been widely reported since osteoclastogenesis and osteolysis are energy-consuming processes[37,38]. Furthermore, the development of ABR is dependent on osteoclastogenesis, which mediates the osteolysis of alveolar bone[39]. In the present study, higher level of glycolysis was shown both in BMDM-derived osteoclasts model and in the rat

alveolar bone tissues of AP-related ABR. HK1 was shown to be a key intracellular enzyme regulating the process of the glycolysis level[10,40], and we reported an important role of HK1-mediated glycolysis in the promotion of osteoclastogenesis in the current study, which contributed to the development of ABR in rat AP model. The above evidence suggests that HK1 regulates glycolysis to promote osteoclastogenesis, which drives ABR in the rat AP model. And the molecular mechanism of HK1 upregulation induced during the development of ABR in rat AP model is intriguing.

m[6]A methylation and demethylation modification are pivotal for genes expression via modulating the gene transcript stability, are associated with the development of multiple diseases[41,42]. In this study, the total levels of m[6]A methylation were downregulated in the development of AP in vivo The expression of the potential target protein
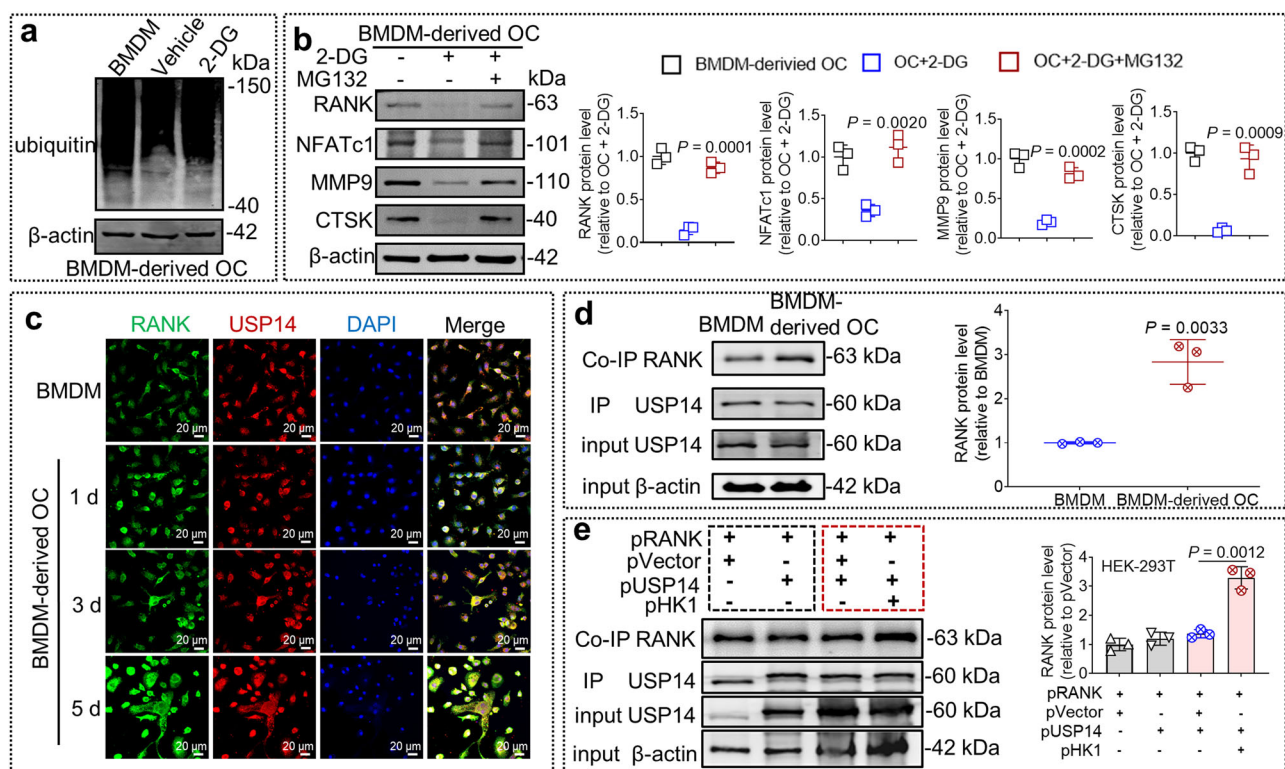
Fig. 10 | HK1 stabilizes RANK protein via USP14 mediated de-ubiquitination of RANK in BMDM-derived osteoclasts. a The relative ubiquitination level in OC after treatment with 0.1 mM 2-DG for 4 days was determined by western blotting ($n = 3$ independent experiments). **b** The relative protein levels of nuclear factor-κB receptor activator (RANK), nuclear factor of activated T cells (NFATc1), matrix metalloprotein 9 (MMP9), and cathepsin K (CTSK) in 2-DG-treated OC after treatment with MG132 (0.5 μM) were determined by western blotting ($n = 3$ independent experiments; mean ± SD). **c** The representative images of RANK (green) and ubiquitin-specific protease 14 (USP14) (red) detection by immunofluorescence in the process of bone marrow macrophage (BMDM)-derived osteoclast (OC). Scale bar indicates 20 μm ($n = 3$ independent experiments). **d** Co-IP assay to examine endogenous interaction between USP14 and RANK in BMDM, and BMDM-derived OC at 5 days ($n = 3$ independent experiments; mean ± SD). **e** Co-IP assay to examine endogenous USP14 and RANK interaction in HEK-293T cells overexpressing RANK after USP14 and hexokinase 1 (HK1) overexpression for 24 h ($n = 3$ independent experiments; mean ± SD). The major statistical procedures applied were: *Shapro–Wiik test* (**b**, **d**, **e**)*, F-test* (**b**, **e**)*, Student-t test* (**d**)*, Kruskal–Wallis H* test and *Dunnett-t test* (**b**, **e**). The statistical test used was two-sided. Source data are available online for this figure.

was modulated by its mRNA m⁶A methylation and demethylation modification[17], and a reduction total m⁶A levels was also observed in HK1 mRNA, suggesting higher level of demethylation activity occurred in HK1 mRNA, promoting HK1 expression, contributing to the development of AP. The m⁶A mRNA demethylase FTO acts as an 'eraser' for m⁶A methylation and further protects the potential target mRNA from degradation under the certain conditions, thus promoting the potential target protein expression[25]. Our biochemical data analysis suggested that FTO was upregulated in BMDM-derived OC and alveolar bone tissue of AP rats. Additionally, He et al. recently reported that FTO was upregulated by inflammatory conditions in the periodontitis[43], and ABR development was associated with infection-induced inflammation, therefore, inflammatory conditions might a specific signal induce FTO expression in during osteoclastogenesis. Furthermore, FTO likely acts directly on HK1 mRNA, and osteoclastogenesis-induced ABR was associated with FTO-mediated m⁶A demethylation modification in HK1 mRNA since FTO knockdown reduced HK1 expression and HK1 expression mediated the glycolysis level. These observations suggest that osteoclastogenesis and ABR development in AP are associated with FTO-mediated HK1 demethylation. Our study was consistent with Zhuang et al., and we found that FTO downregulation inhibited osteoclastogenesis and suppressed the bone resorption[16]. Previous studies had reported a positive regulatory effect of FTO on the glycolysis[18,44]. However, the detailed molecular mechanism of FTO/HK1 regulating osteoclastogenesis remains to be solved.

RANK and its ligand RANKL play a key role in the homeostasis between OC and osteoblasts, while higher level expression of RANK is associated with osteoclastogenesis[29]. As well known, RANK upregulation occurring in the procession of osteoclastogenesis, priming them for further differentiation in response to RANKL[45]. Our data showed that FTO, HK1 and RANK were significantly upregulated during osteoclastogenesis in a time-dependent manner in vitro and in vivo (Figs. 2d, h, 5c, e, 9a), which supported that RANK expression in OC is higher than that expressed in BMDM. Furthermore, FTO/HK1 signal pathway significantly promoted RANK expression during osteoclastogenesis in the alveolar bone tissues of rat AP model. Interestingly, although RANK mRNA was enriched by FTO protein, overexpression FTO alone had a minimal role in the upregulation of exogenous RANK expression. While only FTO and HK1 co-transfection promoted RANK expression, and PKM2-IN-1 (a glycolysis inhibitor acts as a downstream molecule of HK1) abolished the effect of FTO/HK1-mediated RANK upregulation, which implied that the indirect effects of FTO or FTO/HK1 pathway on RANK expression. Furthermore, targeting HK1 inhibition in BMDM-derived osteoclasts downregulated the expression of RANK protein, but not the RANK mRNA, suggesting that the regulation of RANK protein by FTO/HK1 axis occurs at the post-translational rather than the transcriptional stage.

The proteasome pathway has crucial roles in many cellular processes via altering the stability of proteins[46] and has been reported to regulate osteoclastogenesis[47,48]. Unlike ubiquitination activities, deubiquitination protects protein from degradation, which requires the

involvement of deubiquitinating enzymes. Indeed, MG132 treatment reversed an HK1 inhibitor 2-DG-induced degradation of RANK protein, suggesting that the proteasome pathway was involved in the activation of HK1/RANK axis. It would be interesting to illustrate the upstream regulatory mechanism that upregulated RANK expression during osteoclastogenesis. However, we postulate that HK1 is unlikely to be directly associated with the RANK modulation since HKs theoretically have no ubiquitinase activity. Previous studies had reported that HKs expression, especially HK2, was associated with the expression or activation of deubiquitinase, including CSN5[49] and USP11[50]. While the expression of de-ubiquitinase was important for bone homeostasis maintenance[51], for instance, USP26 stabilized β-catenin via its de-ubiquitinase activity to promote the osteogenic activity[52]. Furthermore, de-ubiquitinase POH1 increased osteoclast differentiation[53]. As an isoenzyme of HK2, HK1 has a similar biological function to HK2[54]. USP14 is one of the de-uubiquitinases, who are important for macrophage polarization[33]. It is well known that osteoclast is differentiation from mononuclear macrophages with an activation of RANKL/RANK signaling pathways. At present, a decreased total ubiquitination level was observed in BMDM-derived osteoclasts, and 2-DG partially retraced the total ubiquitination level. Subsequently, USP14 binds to RANK during the process of FTO/HK1-mediated osteoclastogenesis; however, USP14 expression did not change in the process of BMDM-derived osteoclasts. Therefore, we speculate that FTO/HK1/USP14 axis may stabilize RANK expression, resulting in osteoclastogenesis and further involving in the ABR development. Ubiquitination/de-ubiquitination activities require the energy support, and the dysfunction in the glycolytic signaling pathway decreases a balance between the ubiquitination and de-ubiquitination levels[55]. Therefore, we speculate that FTO/HK1 pathway increases the glycolysis level, which provides the energy to support the de-ubiquitination activities, for instance, USP14-mediated RANK de-ubiquitination, which contributes to osteoclastogenesis during the progression of ABR.

However, the axis of FTO/HK1/USP14/RANK was only tested on cell models and animal experiments in our study. Whether the roles of this axis playing in alveolar bone tissues of AP patients also unknown, therefore, the roles of FTO/HK1/USP14/RANK axis should be interpreted with caution in clinical practice, and more studies should be examined in the future.

In summary, the current study revealed a molecular mechanism on osteoclastogenesis-related ABR and found that FTO-mediated HK1 demethylation modification promotes RANK expression via activating USP14-mediated de-ubiquitination activity, which is associated with osteoclastogenesis-induced ABR in AP development. Furthermore, our study demonstrated that treatment with Dac51 (an FTO inhibitor) or/and 2-DG (an HK inhibitor) exhibits a positive effect in delaying the progression of ABR, suggesting that targeting the FTO/HK1/USP14/RANK axis could have the therapeutic implications for AP-related ABR.

Methods

AP-related ABR rat model and AP treatment rat model establishment

All animal experimental protocols were approved by the Animal Ethical and Welfare Committee of Nanjing University (IACUC-D2102040) and followed the 'Guide for the Care and Use of Laboratory Animals' published by the Chinese National Institutes of Health. The research protocols were conducted in accordance with the animal behavioral guidelines, using approved protocols from the institutional animal care committee.

AP-related ABR rat model establishment. The protocol for AP induction was previously described[56,57]. 8-week-old male Wistar rats (Rattus norvegicus, Wistar), weighing 180–220 g of each one, were used in this study. The animals were housed in a temperature-controlled environment (21–25 °C, 70% humidity) with 12 h light/dark cycles, receiving balanced feed (XTI01CR-004, jiangsu Xietong Pharmaceutical Bio-Engineering Co., Ltd) and water. Rats were anesthetized by intraperitoneal injection of 10% ketamine hydrochloride (150 mg/kg of body weight) and 2% xylazine hydrochloride (7.5 mg/kg of body weight). The coronal pulps of the mandibular right first molars were exposed with a spherical carbide bur size 1/4 with 0.5 mm diameter (Dentsply Sirona, Ballaigues, Switzerland) in the mesial fossa of the teeth occlusal, and a K-file (Dentsply Sirona) #15 was introduced to verify the access opening. The pulps were exposed to the oral environment, with the contralateral teeth as control.

AP treatment rat model establishment. 8-week-old male Wistar rats were used to establish a model of AP using the method described above. One week after root canal opening, the rats were randomly assigned to seven groups: PBS, 2-DG (400 mg/kg), Dac51 (2 mg/kg), AAV9-shNC-GFP, AAV9-shHK1-GFP, and AAV9-shFTO-GFP. A #1/2 round bur was used to open the pulp chamber, and the root canals were enlarged by using ProtaperNext (Dentsply Sirona, USA) nickel–titanium endodontic files up to size 25#04 and 2.5 mm in depth. Alternating rinses with 1% NaClO and 17% EDTA solutions, followed by a final rinse with saline by using rinsing needles to simulate standard clinical rinsing procedures. Treated canals were dried using sterilized paper points. Subsequently, PBS, 2-DG, Dac51, AAV9-shNC-GFP, AAV9-shHK1-GFP, and AAV9-shFTO-GFP were injected to the apical area of the mandibular right first molar by microsyringe, and a K-file #15 was used to assist each group of intracanal medicaments to be delivered inside the canal and beyond the apex. Finally, pulp chambers were filled with sterile cotton and sealed with glass–ionomer cement[58]. After 3 weeks, the rats were euthanized with an overdose of isoflurane. The mandibles or the alveolar bone tissues of the mandibular first molar were collected.

Sample collection
The experimental rats were euthanized by an overdose of anesthesia on 1, 3, and 6 weeks after pulp exposure. The mandibles were removed, and stored in 4% paraformaldehyde for 48 h before microcomputed tomography (micro-CT) scanning and further histological processing. Using a surgical microscope, the oral mucosa and teeth were dissected and discarded with a needle holder on the ice. And the alveolar bone tissue around the mandibular first molar was carefully obtained using scissors with 1 mm on the left and right sides of the mandibular first molar as the left and right boundary, and the inferior alveolar canal as the below boundary. Once the alveolar bone tissues have been obtained, they were quickly frozen at −80 °C for the analysis of western blotting and RT–qPCR.

Micro-CT analysis
The mandibles were sectioned in half and scanned in a SkyScan 1176 micro-CT device (Bruker, Kontich, Belgium). The parameters for image acquisition were as follows: 65 kV and 385 μA, with 1 mm thick aluminium filter, exposure time of 340 ms, rotation step of 0.3° and 360° around the vertical axis, and the isotropic resolution at 17 μm. The images were reconstructed using the NRecon software (v1.6.1.0, Bruker) with the following parameters: 4 of ring artefact correction, 40% of beam hardening correction and 2 of smoothing for all images. Image processing and analysis were performed using the CTAn program (v1.6.6.0, Bruker), in an axial view. A manual selection of the region of interest to be evaluated was made in all sets of images, from the first image in which all the roots of the mandibular first molar appeared surrounded by bone crest, until the lesion disappeared[59]. The analysis was performed by a calibrated evaluator. The size of the periradicular lesion was measured, where the area and volume of the lesion were calculated. The CTvox software (v1.6.6.0, Bruker Micro-CT) was used for the three-dimensional visualization of the models.

Tartrate-resistant acid phosphatase staining of tissue sections

The mandibles were fixed in 10% buffered formalin, and demineralized in 10% EDTA, pH 7.4, changed every 3 days for 2 months at room temperature. Subsequently, the samples were paraffin embedded and sectioned at 5 μm (longitudinal and with complete root canals in first mandibular molars). For osteoclast quantification, three consecutive sections per teeth were stained for TRAP using the leukocyte acid phosphatase kit 386A (Sigma-Aldrich, MO, USA). The TRAP-positive (TRAP⁺) cell lining periapical lesion was counted and expressed as the number per millimeter of bone ($n = 9$ per group) as previously described[56,60].

Western blotting analysis

Proteins were isolated from alveolar bone tissues and osteoclast with RIPA buffer on the ice. We used colorimetric Pierce BCA Protein Assay Kit (Thermo Fisher, A65453, MA, USA) with bovine serum albumin (BSA) for generating standard curve and calculate the protein concentration of the sample. Total protein lysates were separated by sodium dodecyl sulfate-polyacrylamide gel electrophoresis (SDS-PAGE) and transferred to polyvinylidene difluoride (PVDF) membrane. The membranes were blocked with 5% BSA for 1 h and individually probed with primary antibodies overnight at 4 °C. Primary antibodies used: nuclear factor-activated T cell 1 (NFATc1, Santa Cruz Biotechnology, Cat#: sc-7294, 1:1000), matrix metalloprotein 9 (MMP9, Proteintech Group, Cat#: 10375-2-AP, 1:1000), cathepsin K (CTSK, Santa Cruz Biotechnology, Cat#: sc-48353, 1:1000), HK1 (Abcam, Cat#: 150423, 1:1000), FTO (Proteintech Group, Cat#: 27226-1-AP, 1:1000), ALKBH5 (Proteintech Group, Cat#: 16837-1-AP, 1:1000), RANK (Bioss, Cat#: 2695R, 1:1000), ubiquitin (Proteintech Group, Cat#: 10201-2-AP, 1:1000), USP14 (Proteintech Group, Cat#: 614517-1-AP, 1:1000) and β-actin (Proteintech Group, Cat#: 66009-1-AP, 1:1000). After washing three times with Tris-buffered saline with 0.1% Tween 20 (TBST), the membranes were incubated with secondary antibodies for 1 h at room temperature. The secondary antibodies were used: IRDye 800 (Goat anti-Mouse) (Rockland, Cat#: 926-32210) and IRDye 680 (Donkey anti-Rabbit IgG)(Rockland, Cat#: 926-68070) and they were purchased from LI-COR (Lincoln, NE, USA). Membranes were scanned using LI-COR Odyssey Imaging System (LI-COR). Image processing was performed using Image Studio Analysis (LI-COR). The uncropped and unprocessed scans of the most important blots in the Source Data file.

RT–qPCR

Total RNA was extracted from the alveolar bone tissues with TRIzol reagent (Invitrogen, CA, USA) according to the manufacturer's instructions. cDNA was obtained by reverse transcription of the RNA samples using a reverse transcription kit (Vazyme Biotech, Nanjing, China). The cDNA was then subjected to RT–qPCR using ABI SYBR Green Master Mix (Life Technologies) on an ABI Prism 7500 sequence detection system. The PCR was carried out using following conditions: 95 °C for 10 min and 40 cycles of 95 °C for 15 s, 60 °C for 10 s, and 72 °C for 15 s, followed by melting curve analysis to confirm primer specificity. The primers are listed in supplementary Table 1. The target gene expression levels were calculated by $2^{-\triangle\triangle CT}$ methods and normalized to β-actin. All reactions were conducted in triplicates.

Cell line and osteoclast culture

Human Embryonic Kidney (HEK-293T) was purchased from National Collection of Authenticated Cell cultures (Cat#: SCSP-502). Bone marrow macrophages (BMDMs) were isolated from tibias and femurs of 6-week-old wild-type mice (C57BL/6). The bones were cut off at both ends and elute into 50 mL conical tubes with α-MEM with 2% FBS and 1% penicillin/streptomycin (Gibco, NY, USA) using 10 mL syringes and 25-G needles. The cell suspension was filtered through a 70 μm cell strainer (BD Biosciences, CA, USA) into a sterile conical tube and centrifuged ($600 \times g$ for 5 min). The pellet was resuspended well in 5 to

10 mL ACK red blood cell lysis buffer (Sigma-Aldrich) for 1 min followed by the addition of α-MEM and centrifugation ($500 \times g$ for 5 min) to terminate the lysis.

Upon red blood cell lysis, BMDMs were cultured overnight (37 °C, 5% CO_2) in α-MEM medium supplemented with 10% FBS, 1% glutamine, 1% penicillin/streptomycin supplemented with 30 ng/mL macrophage colony-stimulating factor (M-CSF, R&D R&D, Cat#: 416-ML-010). The next day, 100,000 non-adherent cells per well were seeded in a 24-well plate with 30 ng/mL M-CSF and 50 ng/mL receptor activator of NF-κB ligand (RANKL, R&D, Cat#: 462-TEC-10) for 4 days. After 4 additional days of culture the cells were stained for TRAP to determine the number of mature OC (TRAP ⁺, ≥3 nuclei).

iTRAQ labeling and data analysis

For each sample ($n = 1$), we added lysis buffer to 120 μg protein until 100 μL, mixed 3 μL trypsin (1 μg/μL), 500 μL (50 mM) TEAB buffer and digested at 37 °C for a night. Equal volume of 1% formic acid (Thermo Fisher) was mixed with digested sample and centrifuged ($12,000 \times g$) for 5 min at room temperature. Extracted the supernatant carefully and loaded to the C18 desalting column (Thermo Fisher), then washed with 1 mL of washing solution which containing 0.1% formic acid and 4% acetonitrile (Thermo Fisher) three times. 0.4 mL washing solution (0.1% formic acid, 4% acetonitrile) was added and eluted twice. When the eluent was dried, 20 μL (1 M) TEAB buffer was added to reconstitute, and mixed with enough iTRAQ labeling using iTRAQ Reagents Multiplex Kit (Sigma-Aldrich) for 2 h at a room temperature. Finally, adding 100 μL (50 mM) Tris-HCl (pH = 8) to stop the reaction, all labeling samples were mixed with an equal volume.

Liquid chromatography-mass spectrometry (LC-MS/MS) analysis was performed on Q ExactiveTM HF-X mass spectrometer (Thermo Fisher) coupled to EASY-nLCTM 1200 UHPLC system (Thermo Fisher) operating in the data-dependent acquisition (DDA) mode. We compared the differentially abundant proteins by using Kyoto Encyclopedia of Genes KEGG genomic pathways were analyzed. For proteins that were differentially enriched in the metabolic pathway of the control group and the 4-week group, were calculated to the base of 2, and the logarithm of p-value was calculated with the base of 10 [61]. The results were then plotted as a volcano plots between the two groups. The mass spectrometry proteomics data have been deposited to the ProteomeXchange Consortium via the iProX partner repository with the dataset identifier PXD059854.

Immunohistochemical (IHC) analysis

Each paraffin tissue block were cut into 3 μm thick tissue sections and placed on slides. IHC analysis was performed using different primary antibodies following the instructions of the manufacturers. After removing the paraffin of slides, they were hydrated in a series of ethanol and then stored in PBS. The tissue sections were microwaved with sodium citrate buffer for the recovery of the antigen. Sections were then rinsed with PBS. After then, the sections were blocked with 3% hydrogen peroxide for 40 min. Furthermore, the sections were blocked with 5% BSA when the slides were washed with PBS. The tissues were then incubated overnight at 4 °C with anti-HK1 primary antibody (Abcam, 150423, 1:100). The slides were then washed and incubated with secondary antibodies for 1 h at room temperature, followed by incubation with streptavidin conjugated to horseradish peroxidase for 20 min. After then, slides were stained with 3,3′-diaminobenzidine for 5 min and then counterstained with haemotoxylin for 15 s.

Immunofluorescence (IF) staining

BMDMs/OC were fixed with 5% paraformaldehyde for 20 min at room temperature and permeabilized with 0.5% Triton X-100 for 15 min. The cells were blocked with 2% BSA for 1 h at room temperature before being incubated with anti-HK1/RANK/FTO/USP14 (1:100 dilution)

antibodies overnight at 4 °C. Antibodies used in western blot as follows: HK1 antibody (Abcam, Cat#: 150423, 1:1000), RANK antibody(Bioss, Cat#: bs-2695, 1:500), FTO antibody(Proteintech Group, Cat#: 27226-1-AP,1:1000), USP14 antibody (Proteintech Group, Cat#: 67746-1-AP, 1:1000). The following day, the cells were incubated with anti-rabbit IgG (Invetrogen, Cat#: A-11012,1:1000) Alexa Fluor 594 or anti-mouse IgG (Invetrogen, Cat#: A-11008, 1:1000) Dylight Fluor 488 with phalloidin for 1 h at room temperature. Finally, DAPI was applied to stain the cell nuclei. Images were collected using an Olympus laser scanning confocal microscope (Olympus, Tokyo, Japan).

Measurement of glucose level
The alveolar bone tissues were ground with a high-speed tissue grinder (Servicebio, Wuhan, China). After centrifugation at $835 \times g$ for 10 min, the supernatant was collected, and then the glucose level was measured using the Automatic Biochemical Analyzer (Biobase, Shandong, China, ADS-W-TDX040). All values were normalized to the protein concentration[10].

Measurement of pyruvate and lactate levels
The alveolar bone tissues were ground with a high-speed tissue grinder (Servicebio, Wuhan, China). After centrifugation at $580 \times g$ for 10 min, the supernatant was collected, and pyruvate and lactate levels were measured by a Pyruvate Assay Kit (Jiancheng, Nanjing, China, Cat#: A081) and Lactate Assay Kit (Jiancheng, Nanjing, China, Cat#: A019-2) according to the manufacturer's instructions. The results were measured at a wavelength of 505 nm or 530 nm using a SpectraMax M5 multifunctional microplate reader (BD Falcon, CA, USA) to determine pyruvate or lactate levels, respectively.

Hexokinase activity assay
The alveolar bone tissues were ground with lysis buffer, then centrifuged at $12,000 \times g$ for 10 min at 4 °C. Supernatants were incubated and HK activity was determined with HK Assay Kit (Biobase, Shandong, China, Cat#: ADS-W-T001) following G6PD-dependent conversion of $NADP^+$ to NADPH spectrophotometrically at 340 nm. The values were normalized to the protein concentration.

Measurement of extracellular acidification rate
Seahorse XF^{e}96 analyzer (Seahorse Bioscience, Agilent, Santa Clara, CA) was used to measure the extracellular acidification rate (ECAR) based on the manufacture's protocols[62]. Briefly, 100,000 BMDMs were seeded in each well and cultured 4 days in XF assay medium supplemented with 30 ng/mL M-CSF (R&D, Cat#: 416-ML-010) and 50 ng/mL RANKL(R&D, Cat#: 462-TEC-10). Culturing media was changed with the modified DMEM media and placed into a 37 °C non-CO_2 incubator for 1 h. After preparation of drugs and XF Cell Mito Stress Test Kit (Agilent, Cat#: 103020-100) and glycolytic rate kit (Seahorse Bioscience) into cartridge ports, the cartridge and cell culture plates were loaded into XF96 analyzer (Seahorse Bioscience)[63]. Experiments were performed in triplicates.

Cell counting 8 kit (CCK-8) assay
After the BMDM had adhered, various concentrations of Dac51 (Selleck, Houston, USA, Cat#: S9876)/2-DG (MCE, NJ, USA, Cat#: HY-13966) were added, and the cells were incubated for 24 h in 96-well culture plates. Next, the cells were incubated in the dark for 4 h at 37 °C with 10 µL of CCK-8 reagent (Vazyme Biotech, Nanjing, China, Cat#: A311). The results were determined by measuring the absorbance at a wavelength of 450 nm using a SpectraMax M5 multifunctional microplate reader.

Vector construction, transfection, and lentivirus transduction
ShRNA with sequences complementary to HK1 or/and FTO was subcloned into the LV3 lenti-viral vector. The nucleotide sequence of shRNA-

HK1 (Lenti-shHK1) is CGTAGACGGTTCTCTCTACAA. The nucleotide sequence of shRNA-FTO (Lenti-shFTO) is GTCTCGTTGAAATCCTTTGAT. Recombinant lentivirus containing HK1/FTO shRNA were produced in HEK-293T cells. The lentivirus-containing supernatant was harvested 48 h after transfection and filtered through a 0.45 µm filter (Millipore, MA, USA). The recombinant lentivirus was concentrated at $25,000 \times g$ for 2 h.

Production of the multi-shRNA RNAi vector targeting HK1 or/and FTO
The designated AAV9-CD68-3×shRNAHK1 or AAV9-CD68-3×shRNAFTO are obtained from Shanghai Genechem Co., Ltd. Three target sites for silencing the HK1 were designed. These sequences were as follows: 5'-TGTGGTCAAGTTGCTGAATAA-3', 5'-GGAATTTGACTTG-GATGTGGT-3' and 5'-TGGGTTTGAACAGCACGTGTG-3'. Three target sites for silencing the FTO were designed. These sequences were as follows: 5'-TTGGAAGAACTGGCTATCAAA-3', 5'-AGGCTTGACAAT TCCTCTTCA-3' and 5'-TGCCGTGCTTCGTGAAGTTAA-3'. The adeno-associated virus vector expressing short hairpin RNA (shRNA) targeting the sequence of HK1 gene or/and FTO gene and negative control (TTCTCCGAACGTGTCACGT) were synthesized and cloned into CV232 (pAAV-CD68-EGFP-3×Flag-mir155(rHK1)-WPRE-SV40-ploya) vector or/and (pAAV-CD68-EGFP-3×Flag-mir155(rFTO)-WPRE-SV40-ploya) with BsmBI sites (purchased from Shanghai Genechem Co., Ltd) and then recombinant vector was detected by DNA sequencing. According to the previous studies from Grace et al., and Lu et al., CD68 was selected as the promoter, which is uniquely expressed in macrophages[64,65]. Therefore, HK1 or FTO under a CD68 (specific for macrophage) promoter were transfected via an AAV9 vector.

Adeno-associated virus production
The viral vector were transfacted into HEK-293T cells using Lipofectamine 2000 (Invitrogen; Cat#: 11668019) together with plasmids pHelper and pRepCap. Adeno-Associated Virus were harvested 72 h post transfection, AAV9 were purified through iodixanol gradient ultracentrifuge and subsequent concentration. Purified AAV viruses were tittered using a quantitative PCR-based method.All AAV used in this study was prepared in 0.001% Pluronic F-68 solution (Poloxamer 188 Solution, PFL01-100 mL, Caisson Laboratories, Smithfield, UT, USA).

Resorption assay
BMDMs were seeded on bone disks (Boneslices) in 96-well plates with osteoclastogenic media containing recombinant M-CSF (30 ng/mL) and RANKL (50 ng/mL). After 4 d, OC were removed from the bone slices, and resorption events were stained with toluidine blue (GENMED). Images were collected using a magnifying glass (Leica MZ6), and all resorption events were distinguished into pits.

Dot-blot assay
Total RNA was extracted with Trizol reagent and the quality and quantity of RNA were assessed by NanoDrop 2000 (Thermo Fisher). The RNA was diluted with DEPC to the final concentration of 100 ng/µL. 2 µL of RNA was denatured by heating at 95 °C for 3 min, then chilling on ice immediately to prevent the secondary structure of mRNA from re-forming. Next, RNA was spotted on nitrocellulose filter membranes and cross-linked to the membrane at 37 °C for 30 min. The membranes were blocked with 5% BSA in TBST and the total m^{6}A level was detected by using the m^{6}A-specific antibody (Beyotime, AF7407, 1:500). After extensive washing, the membranes were incubated with IRDye 680 donkey-anti-rabbit (Rockland, Cat#: 926-68070) or IRDye 800 goat-anti-mouse (Rockland, Cat#: 926-32210) at room temperature for 1 h and then scanned using LI-COR Odyssey Imaging System.

RNA binding protein immunoprecipitation (RIP) assay

RIP assay was performed according to the instructions of Magnetic RNA-Protein Pull-Down Kit (Thermo Fisher). The alveolar bone tissues or OC were lysed with RIP lysis buffer supplemented with RNase inhibitor and protease inhibitor cocktail. Magnetic beads were incubated with RIP wash buffer for 30 min and antibodies to prepare bead-antibody complex. Cell lysis was immunoprecipitated with m^6A/FTO or control IgG at 4 °C overnight, followed by RNA purification. Finally, the immunoprecipitated RNA was analyzed by RT-qPCR.

Plasmid transfection

293T cells were grown in DMEM medium supplemented with 10% FBS. For transfection, pFTO (Miaoling, Cat#: P41507)/pHK1 (Miaoling, Cat#: P27233)/pRANK (Miaoling, Cat#: P59532) were transfected into cells using Lipofectamine 8000 reagent (Beyotime, Cat#: C0533) according to the manufacturer's instructions. The cells were collected after 24 h.

RNA stability assay

Transfected 293T cells were incubated with the transcriptional inhibitor Actinomycin D (MCE, Cat#: HY-17599) (5 µg/mL) at 0 h, 3 h, 6 h, 9 h. The total RNA from the cells was isolated by TRIzol Reagent. The remaining expression of HK1 mRNA for each group was calculated using qPCR analysis.

Oxygen consumption rates (OCR)

Seahorse XF^{e}96 analyzer was used to measure the oxygen consumption rates (OCR) based on the manufacture's protocols. Briefly, 100,000 BMDMs were seeded in each well and cultured 4 days in XF assay medium supplemented with 30 ng/mL M-CSF, 50 ng/mL RANKL and lenti-shFTO. Culturing media was changed to modified DMEM media and placed into a 37 °C non-CO_2 incubator for 1 h. Interval injections of 1 µM oligomycin, 1 µM FCCP and 0.5 µM rotenone/antimycin A were for determining the OCR. After preparation of drugs and XF Cell Mito Stress Test Kit (Agilent, Cat#: 103015-100) into cartridge ports, the cartridge and cell culture plates were loaded into XF96 analyzer (Seahorse Bioscience). Experiments were performed in triplicates.

Co-immunoprecipitation (Co-IP)

Immunoprecipitation was performed using an anti-USP14 antibody (IP: USP14) or IgG (IP: IgG) After washing with PBS, the cells with Co-IP buffer (50 mM Tris-HCl [pH 7.4], 150 mM NaCl, 2 mM EDTA, 1 % NP-40, 10 % glycerol, 1 mM DTT, 1 mM PMSF), followed by a centrifugation at $12,000 \times g$ for 10 min at 4 °C. Subsequently, 5 µg of the indicated antibody or IgG was added to the supernatants and incubated overnight at 4 °C, followed by incubation with 60 µl protein A/G agarose for 2 h at 4 °C to form agarose-antibody-protein complexes. The beads were then washed three times with Co-IP buffer and eluted with 1 × SDS loading buffer and then boiled for 5 min. The pulled-down proteins were separated by SDS-PAGE and subsequently analyzed via western blotting.

Statistical analysis and reproducibility

Quantitative data supporting our study are presented as mean ± standard deviation (SD) and were analyzed using GraphPad Prism 9.0 software (GraphPad, San Diego, CA, USA) or SPSS 21.0 statistical software (IBM Corporation, USA). All data were initially determined to be normally distributed or not by the *Shapro−Wiik* test. For data that conforms to a normal distribution, comparisons between two groups were analyzed using two-tailed Student's *t*-test or paired *t*-test. *One-way ANOVA or Repeated measures ANOVA* followed by *Dunnett'-t* test and *SNK-q* test were used to compare more than two data groups, which were run only if *F*-test achieved $P > 0.05$, and there was no significant variance in homogeneity. Nonparametric tests were used for data sets that did not conform to a normal distribution or with *F*-test $P < 0.05$: *Kruskal−Wallis H* test was used to compare more than two data groups. *Wilcoxon* test was used to compared the repeated measures data of the two groups or the two independent samples. As for the choice of sample size, we reviewed the sample size of similar studies and conducted preliminary experiments to estimate effect size and data variability. The experiments were repeated independently at least three times with similar results unless otherwise mentioned, and the micrographs were the representative data from individual samples (the n was provided in figure legends). The investigators were not blinded to group allocation during data collection and /or analysis in this study.

Reporting summary

Further information on research design is available in the Nature Portfolio Reporting Summary linked to this article.

Data availability

All data supporting the findings described in this manuscript are available in the article and in the Supplementary Information and from the corresponding author upon request and the source data are provided with this paper. The mass spectrometry proteomics data have been deposited to the ProteomeXchange Consortium via the iProX partner repository with the dataset identifier PXD059854. Source data are provided with this paper.

References

1. Leng, S. et al. NLRP3 disturbs Treg/Th17 cell balance to aggravate apical periodontitis. *J. Dent. Res.*, 220345231151692, https://doi.org/10.1177/00220345231151692 (2023).
2. Jakovljevic, A. et al. Involvement of the Notch signaling system in alveolar bone resorption. *Jpn. Dent. Sci. Rev.* **59**, 38–47 (2023).
3. Deng, Z., Lin, B., Liu, F. & Zhao, W. Role of Enterococcus faecalis in refractory apical periodontitis: from pathogenicity to host cell response. *J. Oral. Microbiol.* **15**, 2184924 (2023).
4. Sadek, K. M. et al. Molecular basis beyond interrelated bone resorption/regeneration in periodontal diseases: a concise review. *Int. J. Mol. Sci.* **24**, https://doi.org/10.3390/ijms24054599 (2023).
5. Tsuchida, S. & Nakayama, T. Recent clinical treatment and basic research on the alveolar bone. *Biomedicines* **11**, https://doi.org/10.3390/biomedicines11030843 (2023).
6. Sakuraba, K. et al. Autoantibodies targeting malondialdehyde-modifications in rheumatoid arthritis regulate osteoclasts via inducing glycolysis and lipid biosynthesis. *J. Autoimmun.* **133**, 102903 (2022).
7. Da, W., Tao, L. & Zhu, Y. The role of osteoclast energy metabolism in the occurrence and development of osteoporosis. *Front. Endocrinol.* **12**, 675385 (2021).
8. Mlozen, M. M., Van Marwijk, J., Wilhelmi, B. S. & Whiteley, C. Comparative analysis of the interaction of silver nanoparticles with hexokinase from Trypanosoma brucei and humans. *Int. J. Nanomed.* **18**, 1399–1411 (2023).
9. Lauterwasser, J. et al. Hexokinases inhibit death receptor-dependent apoptosis on the mitochondria. *Proc. Natl Acad. Sci. USA* **118**, https://doi.org/10.1073/pnas.2021175118 (2021).
10. Qian, Y. et al. Targeting hexokinase 1 alleviates NLRP3-mediated inflammation in apical periodontitis: a laboratory investigation. *Int. Endod. J.* https://doi.org/10.1111/iej.13913 (2023).
11. Liu, X. S. et al. Comprehensive analysis of hexokinase 2 immune infiltrates and m6A related genes in human esophageal carcinoma. *Front. Cell Dev. Biol.* **9**, 715883 (2021).
12. Yuan, B. & Zhou, J. N6)-methyladenosine (m(6)A) reader IGF2BP1 facilitates clear-cell renal cell carcinoma aerobic glycolysis. *PeerJ* **11**, e14591 (2023).
13. Huang, M. et al. m6A methylation regulates osteoblastic differentiation and bone remodeling. *Front. Cell Dev. Biol.* **9**, 783322 (2021).
14. Li, D., Cai, L., Meng, R., Feng, Z. & Xu, Q. METTL3 modulates osteoclast differentiation and function by controlling RNA stability

and nuclear export. *Int. J. Mol. Sci.* **21**, https://doi.org/10.3390/ijms21051660 (2020).

15. Qiao, Y. et al. Identification and experimental validation of key m6A modification regulators as potential biomarkers of osteoporosis. *Front. Genet.* **13**, 1072948 (2022).

16. Zhuang, J. et al. Downregulated fat mass and obesity-associated protein inhibits bone resorption and osteoclastogenesis by nuclear factor-kappa B inactivation. *Cell Signal* **87**, 110137 (2021).

17. Huang, J. et al. FTO suppresses glycolysis and growth of papillary thyroid cancer via decreasing stability of APOE mRNA in an N6-methyladenosine-dependent manner. *J. Exp. Clin. Cancer Res.* **41**, 42 (2022).

18. Zhang, B. et al. m6A demethylase FTO attenuates cardiac dysfunction by regulating glucose uptake and glycolysis in mice with pressure overload-induced heart failure. *Signal Transduct. Target Ther.* **6**, 377 (2021).

19. Udagawa, N. et al. Osteoclast differentiation by RANKL and OPG signaling pathways. *J. Bone Miner. Metab.* **39**, 19–26 (2021).

20. Ethiraj, L. P. et al. Colorimetric and fluorescent TRAP assays for visualising and quantifying fish osteoclast activity. *Eur. J. Histochem.* **66**, https://doi.org/10.4081/ejh.2022.3369 (2022).

21. Willbold, E. & Witte, F. Histology and research at the hard tissue-implant interface using Technovit 9100 New embedding technique. *Acta Biomater.* **6**, 4447–4455 (2010).

22. De Jesus, A. et al. Hexokinase 1 cellular localization regulates the metabolic fate of glucose. *Mol. Cell* **82**, 1261–1277 e1269 (2022).

23. Wang, F. F. et al. KLF2 mediates the suppressive effect of BDNF on diabetic intimal calcification by inhibiting HK1 induced endothelial-to-mesenchymal transition. *Cell. Signal.* **94**, 110324 (2022).

24. Wang, T., Kong, S., Tao, M. & Ju, S. The potential role of RNA N6-methyladenosine in Cancer progression. *Mol. Cancer* **19**, 88 (2020).

25. Mathiyalagan, P. et al. FTO-dependent N(6)-methyladenosine regulates cardiac function during remodeling and repair. *Circulation* **139**, 518–532 (2019).

26. Liu, Y. et al. Tumors exploit FTO-mediated regulation of glycolytic metabolism to evade immune surveillance. *Cell Metab.* **33**, 1221–1233 e1211 (2021).

27. Qing, Y. et al. R-2-hydroxyglutarate attenuates aerobic glycolysis in leukemia by targeting the FTO/m(6)A/PFKP/LDHB axis. *Mol. Cell* **81**, 922–939 e929 (2021).

28. Wu, L. et al. Aspirin inhibits RANKL-induced osteoclast differentiation in dendritic cells by suppressing NF-κB and NFATc1 activation. *Stem Cell Res. Ther.* **10**, 375 (2019).

29. Boyle, W. J., Simonet, W. S. & Lacey, D. L. Osteoclast differentiation and activation. *Nature* **423**, 337–342 (2003).

30. Yoshimoto, T. et al. Osteocytes directly regulate osteolysis via MYD88 signaling in bacterial bone infection. *Nat. Commun.* **13**, 6648 (2022).

31. Huang, X., Liang, Y., Qing, Y., Chen, D. & Shi, N. Proteasome inhibition by MG-132 protects against deltamethrin-induced apoptosis in rat hippocampus. *Life Sci.* **220**, 76–83 (2019).

32. Wei, D., Tian, X., Ren, Z., Liu, Z. & Sun, C. Mechanistic insights into the role of USP14 in adipose tissue macrophage recruitment and insulin resistance in obesity. *Int. J. Biol. Macromol.* **267**, 131645 (2024).

33. He, F., Chen, Y., He, D. & He, S. USP14-mediated deubiquitination of SIRT1 in macrophage promotes fatty acid oxidation amplification and M2 phenotype polarization. *Biochem. Biophys. Res. Commun.* **646**, 19–29 (2023).

34. Wu, J. et al. Folate metabolism negatively regulates OAS-mediated antiviral innate immunity via ADAR3/endogenous dsRNA pathway. *Metabolism*, 155526, https://doi.org/10.1016/j.metabol.2023.155526 (2023).

35. Wu, J. et al. FOLR1-induced folate deficiency reduces viral replication via modulating APOBEC3 family expression. *Virol. Sin.* https://doi.org/10.1016/j.virs.2023.04.001 (2023).

36. Ho, T., Potapenko, E., Davis, D. B. & Merrins, M. J. A plasma membrane-associated glycolytic metabolon is functionally coupled to K(ATP) channels in pancreatic α and β cells from humans and mice. *Cell Rep.* **42**, 112394 (2023).

37. Li, B. et al. Both aerobic glycolysis and mitochondrial respiration are required for osteoclast differentiation. *FASEB J.* **34**, 11058–11067 (2020).

38. Lemma, S. et al. Energy metabolism in osteoclast formation and activity. *Int. J. Biochem. Cell Biol.* **79**, 168–180 (2016).

39. Jayusman, P. A. et al. Overview on postmenopausal osteoporosis and periodontitis: The therapeutic potential of phytoestrogens against alveolar bone loss. *Front. Pharm.* **14**, 1120457 (2023).

40. Chen, Q. T. et al. HK1 from hepatic stellate cell-derived extracellular vesicles promotes progression of hepatocellular carcinoma. *Nat. Metab.* **4**, 1306–1321 (2022).

41. Deng, X., Qing, Y., Horne, D., Huang, H. & Chen, J. The roles and implications of RNA m(6)A modification in cancer. *Nat. Rev. Clin. Oncol.* https://doi.org/10.1038/s41571-023-00774-x (2023).

42. Liu, Y. et al. N6-methyladenosine-mediated gene regulation and therapeutic implications. *Trends Mol. Med.* **29**, 454–467 (2023).

43. He, J. et al. FTO regulates osteoclast development by modulating the proliferation and apoptosis of osteoclast precursors in inflammatory conditions. *Cell Signal* **117**, 111098 (2024).

44. Zhang, Y. et al. PRKAA1, stabilized by FTO in an m6A-YTHDF2-dependent manner, promotes cell proliferation and glycolysis of gastric cancer by regulating the redox balance. *Neoplasma* **69**, 1338–1348 (2022).

45. Boyce, B. F. Advances in the regulation of osteoclasts and osteoclast functions. *J. Dent. Res.* **92**, 860–867 (2013).

46. Yalçin, Z. et al. Ubiquitinome profiling reveals in vivo UBE2D3 targets and implicates UBE2D3 in protein quality control. *Mol. Cell Proteomics* 100548, https://doi.org/10.1016/j.mcpro.2023.100548 (2023).

47. Ethiraj, P. et al. Proteasome inhibition suppress microgravity elevated RANK signaling during osteoclast differentiation. *Cytokine* **125**, 154821 (2020).

48. Zeng, R. et al. E3 ubiquitin ligases: potential therapeutic targets for skeletal pathology and degeneration. *Stem Cells Int.* **2022**, 6948367 (2022).

49. Huang, M., Xiong, H., Luo, D., Xu, B. & Liu, H. CSN5 upregulates glycolysis to promote hepatocellular carcinoma metastasis via stabilizing the HK2 protein. *Exp. Cell Res.* **388**, 111876 (2020).

50. Wang, J. et al. A non-metabolic function of hexokinase 2 in small cell lung cancer: promotes cancer cell stemness by increasing USP11-mediated CD133 stability. *Cancer Commun.* **42**, 1008–1027 (2022).

51. Guo, Y. C., Zhang, S. W. & Yuan, Q. Deubiquitinating enzymes and bone remodeling. *Stem Cells Int.* **2018**, 3712083 (2018).

52. Li, C. et al. The osteoprotective role of USP26 in coordinating bone formation and resorption. *Cell Death Differ.* **29**, 1123–1136 (2022).

53. de Poot, S. A. H., Tian, G. & Finley, D. Meddling with fate: the proteasomal deubiquitinating enzymes. *J. Mol. Biol.* **429**, 3525–3545 (2017).

54. Zapater, J. L., Lednovich, K. R., Khan, M. W., Pusec, C. M. & Layden, B. T. Hexokinase domain-containing protein-1 in metabolic diseases and beyond. *Trends Endocrinol. Metab.* **33**, 72–84 (2022).

55. Chen, X., Htet, Z. M., López-Alfonzo, E., Martin, A. & Walters, K. J. Proteasome interaction with ubiquitinated substrates: from mechanisms to therapies. *FEBS j.* **288**, 5231–5251 (2021).

56. Taira, T. M. et al. NLRP12 attenuates inflammatory bone loss in experimental apical periodontitis. *J. Dent. Res.* **98**, 476–484 (2019).

57. Justo, M. P. et al. Curcumin reduces inflammation in rat apical periodontitis. *Int. Endod. J.* **55**, 1241–1251 (2022).

58. Siddiqui, Y. D. et al. Resolvin D2 induces resolution of periapical inflammation and promotes healing of periapical lesions in rat periapical periodontitis. *Front. Immunol.* **10**, 307 (2019).

59. Pinto, K. P. et al. Effects of alcohol and nicotine consumption on the development of apical periodontitis in rats: a correlative micro-computed tomographic, histological and immunohistochemical study. *Int. Endod. J.* **53**, 1238–1252 (2020).

60. Fukada, S. Y. et al. iNOS-derived nitric oxide modulates infection-stimulated bone loss. *J. Dent. Res.* **87**, 1155–1159 (2008).

61. Xu, Q. et al. iTRAQ-based proteomic analysis reveals proteins associated with cold stress response in two different populations of Manila clam (Ruditapes philippinarum). *Proteomics* e2100396, https://doi.org/10.1002/pmic.202100396 (2023).

62. Sheng, G. et al. P2RX7 promotes osteosarcoma progression and glucose metabolism by enhancing c-Myc stabilization. *J. Transl. Med.* **21**, 132 (2023).

63. Drummer, C. T. et al. Caspase-11 promotes high-fat diet-induced NAFLD by increasing glycolysis, OXPHOS, and pyroptosis in mac-rophages. *Front. Immunol.* **14**, 1113883 (2023).

64. Grace, P. M. et al. DREADDed microglia in pain: Implications for spinal inflammatory signaling in male rats. *Exp. Neurol.* **304**, 125–131 (2018).

65. Lu, Y. et al. DEL-1 suppression attenuates atherosclerosis by mod-ulating macrophagic GSK-3β/CEBP-β signaling pathway. *Int. J. Cardiol.* **376**, 115–124 (2023).

Author contributions

Y.Q., J.W., and D.C. conducted the most experiments, analyzed the data and wrote the draft manuscript and revised the manuscript. W.Y., D.C. and Y.Zhu provided the technical assistance and financially supported the study. R.L., Q.Y., J.L., Q.H., and Y. Zhuang. did the animal experi-ments. W.W., Y.W., Y. Zhu., and Z.W. monitored the project administra-tion. All authors critically read the article and approved the final version.

Competing interests

The authors declare no competing interests.

Additional information

Supplementary information The online version contains supplementary material available at https://doi.org/10.1038/s41467-025-56615-1.

Correspondence and requests for materials should be addressed to Wenmei Wang, Yong Wang, Yanan Zhu, Zhiwei Wu or Deyan Chen.

Peer review information *Nature Communications* thanks Hongchang Lai and the other anonymous reviewer(s) for their contribution to the peer review of this work. A peer review file is available.

Reprints and permissions information is available at http://www.nature.com/reprints

Publisher's note Springer Nature remains neutral with regard to jur-isdictional claims in published maps and institutional affiliations.